Identification of Inhibiting Factors of a Null Significant Tornado Event

Joshua M. Boustead
National Weather Service Forecast Office Omaha, Nebraska

Philip N. Schumacher
National Weather Service Forecast Office Sioux Falls, South Dakota

Date of Submission: February 21st, 2007

Corresponding author address: Joshua M. Boustead, National Weather Service, 6707 N. 288th Street, Valley, NE 68064. E-mail: josh.boustead@noaa.gov

Abstract

A significant tornado outbreak was forecast over a large portion of the Central and Northern Plains on 5 June 1999. The outbreak was forecast to develop ahead of a strong upper-level cyclone moving through the central Rocky Mountains, in an atmosphere characterized by strong deep-layer shear and extreme instability. Although severe weather did occur, and some of the activity was significant, in most of the high risk area only isolated tornadoes were observed. This study will show that despite favorable deep shear and instability, mesoscale and storm-scale forcing was unable to overcome a pronounced lack of favorable synoptic scale dynamic support. This maintained a persistent capping inversion, and likely prevented a significant tornado outbreak. The lack of favorable dynamic support is related to the passage of a migratory short-wave ridge over the risk area during peak heating. The absence of large-scale ascent associated with the short-wave ridge is identified using several tools, including 3-hourly RUC model analyses, 6-hourly radiosondes, and visible and water vapor satellite images. The 6 and 12 hour NCEP numerical model guidance available to operational forecasters at 1200 UTC 5 June will also be compared to the observational data to show the evolution of the thermodynamic differences that developed during the period. This

null significant tornado event offered an excellent opportunity to identify possible inhibiting factors that prevented a significant tornado outbreak.

1. Introduction

The interest and subsequent research in the area of severe local storms has significantly increased over the past 50 years. This has led to the improvement of conceptual models for anticipating severe weather, better tools for assessing real-time information (e.g. GOES satellite, WSR-88D radars), and additional parameters to help assess the type of severe weather most likely to occur (e.g. Bulk Richardson Number Shear, Energy Helicity Index, Storm Relative Helicity; see Rasmussen 2003 for more details). Much of the published research to date has concentrated on the evolution of severe local storms once they have developed, or events that were not forecast (Edwards et al. 2001), but not on the process of convective initiation. In particular, there has been only a limited amount of published research involving cases where severe local storms appeared likely but failed to develop (null case studies) (Doswell et al. 2002).

For the purpose of this study, a "null event" will be defined as a non-occurrence of any forecasted weather element. In the case of 5 June 1999 a regional tornado outbreak was forecast by the National Oceanic and Atmospheric Administration (NOAA) Storm Prediction Center (SPC), including the risk of "large and destructive tornadoes" (Fig. 1). Although severe weather, including tornadoes, did occur in the highest risk area, only two of the tornadoes reached F1 strength (Fujita 1981), with the rest of the tornadoes surveyed at F0 intensity (Storm Data 1999).

In addition, the tornadoes that occurred were confined to a small geographical area generally outside the high risk delineated by SPC. A plot of the documented severe weather reports on 5 June is presented in Figure 2. The majority of the severe weather reports were near an inverted trough, and south of a synoptic cold front. A lack of significant severe weather events is noted across central and southern Nebraska and all of Kansas. The fact that a significant tornado outbreak was forecast and did not materialize provides a unique opportunity to study where current conceptual models used for tornado forecasting failed, and how the results can be applied to future events.

A limited amount of published research has been done in the area of null event cases. This research is critical to better understand what factors can inhibit severe weather. A better understanding of these factors may enable forecasters to reduce the false alarm rate, and in return, elicit better preparedness and response from customers when severe weather is forecast. Doswell (1987; hereafter D87) presented a case of a marginal severe weather threat on 6 May 1983 where the initiation of convection was not certain due to a strong capping inversion and only modest amount of low-level moisture present. D87 suggested that the initiation of thunderstorms was a mesoscale process, and the occurrence of large-scale severe weather outbreaks is most likely when the synoptic and mesoscale environment favor severe weather development (McNulty 1995). On 6 May 1983 the synoptic scale environment was marginally favorable for the development of severe weather, but the mesoscale forcing was able to overcome the inhibiting factors provided by the synoptic environment (the capping inversion and marginal moisture) and produce intense convection.

A study by Richter and Bosart (2002; hereafter RB02) looked at the suppression of deep moist convection along the dryline in the Southern Plains. In RB02, a detailed data set was available for examination of the convective environment due to the operation of The Verification of the Origins of Rotation (VORTEX; Rasmussen et al. 1994)[1]. In their study thunderstorms were expected to develop and become tornadic in a targeted area of the Texas panhandle during the afternoon and evening. There was no convective initiation in the targeted area during the time frame. The forecast error was hypothesized to have been caused by poor initialization of the available forecast models due to observational data voids over northern Mexico and the Pacific Ocean.

In another null severe weather event Doswell et al. (2002; hereafter D02) presented a case where isolated tornadic supercells were expected. Thunderstorms did develop due to a favorable synoptic scale environment, but mesoscale processes limited the tornado potential. In this case the supercell was only able to produce tornadoes in a narrow axis of high Θ_e air over extreme eastern New Mexico. The inhibiting factor appeared to be earlier convection in the Texas Panhandle that produced a region of high static stability near the surface due to persistent cloud cover along an outflow boundary. As the supercell encountered this hostile surface environment, it become elevated above the cool stable boundary layer and no longer produced tornadoes.

As discussed in D02, the threat for severe weather, including tornadoes, exists on many days across the central Great Plains during the spring and summer. However, severe weather often fails to materialize even when conditions appear supportive of such development. A study

[1] Only meteorological data available to operational forecasters on 5 June 1999 was used for the case study. This was done in an attempt to relate this event to operational forecasters, and what information was available during the evolution of the convective environment on 5 June.

of verification of tornado watches issued by the SPC from 1967 to 1990 indicated an increase of watches verified with tornadoes from 30 to 53% (Anthony and Leftwich 1992). Although significant, there is also a significant amount of watches that are not verified by tornadoes. Therefore it is important for operational forecasters to recognize inhibiting factors which could reduce the potential for severe thunderstorms. In addition, nearly 67% of tornado-related deaths are associated with significant tornadoes (defined as a tornado with F2 strength or greater; Concannon et al. 2000). This makes the distinction of strong and violent tornado days from weak tornado days critical for operational forecasters.

D02 noted that factors that inhibit convection can occur on the mesoscale and even the storm scale; this case study identifies inhibiting factors that occurred on the synoptic scale. These inhibiting factors had direct impact on the ability of the mesoscale, and ultimately the storm scale, to produce widespread convection. The goal of this study is to determine factors that may have prevented the expected significant severe weather event from occurring. Since one cannot know conclusively what the outcome would have been in the absence of inhibiting factor(s) in this paper, inferences made from the observational data will be used to support the conclusions of the study.

A methodology is presented in section 2. A detailed analysis of the synoptic environment is presented in section 3. Possible inhibiting factors are identified in section 4. Section 5 covers the forecasting of the event. Finally in section 6, conclusions are provided that discuss lessons to be learned from this event and how these lessons can be applied to operational forecasting.

2. Methodology

Observed upper air and surface data were obtained and subjectively analyzed for 5 and 6 June 1999. The upper air data were objectively analyzed to a 1° x 1° latitude and longitude using the Barnes objective analysis scheme within the General Meteorological Package software (GEMPAK; DesJardins et al. 1991). Surface data were objectively analyzed to a 0.5° x 0.5° grid. Both objectively analyzed data sets were used to compute derived quantities such as vertical motion and moisture convergence. Operational numerical model data were also obtained for the Nested Grid Model (NGM), Eta (Rogers et al. 1996), aviation model (AVN), and Rapid Update Cycle (RUC) model (Benjamin et al. 2004). Data was available from 0000 UTC 5 June through 0000 UTC 6 June. All data were reanalyzed to an 80 km grid every 50 hPa from 1000 hPa to 100 hPa. To calculate Q-vectors and divergence of Q-vectors, the gridded data were then smoothed to remove most mesoscale waves using the filter described by Barnes et al. (1996). The RUC model initialized analysis was available every 6 hours, and was assumed to be generally representative of the actual environment to be used in comparison with data from the other operational models (Thompson and Edwards 2000).

3. Synoptic Discussion

a. Upper air analysis

Subjective upper air analyses valid at 1200 UTC 5 June 1999 are presented in Figure 3. At 300 hPa, a deep trough and associated jet maximum were located over the southern Rocky Mountains (Fig. 3a). The strongest jet segment was positioned over New Mexico and was beginning to eject to the northeast. At 500 hPa, a closed upper-level low was located over eastern Utah with unseasonably cold air of -20°C (Fig. 3b). The synoptic pattern included a large-scale

ridge extending from the lower Mississippi River valley into the Great Lakes. Two distinct shortwave troughs are visible at 1200 UTC, one over the eastern Dakotas and western Minnesota, and the other over southern Colorado and New Mexico both are associated with 30+ m s^{-1} speed maxima. A thermal ridge of +12 to +15 °C at 700 hPa, representative of the elevated mixed layer (EML) extended from southwest Texas into Nebraska and Iowa (Fig. 3c). The EML capped a moist, potentially unstable boundary layer. The relatively deep moisture, indicated by the 850 hPa moisture axis, extended from southwest Texas into the western Great Lakes (Fig. 3d).

At 0000 UTC 6 June 1999, the subjective upper air analyses indicated that the 300 hPa jet maximum, which was over New Mexico at 1200 UTC, had lifted into the High Plains from Kansas into the Texas Panhandle (Fig. 4a). At 500 hPa, the upper-level closed low had moved into Colorado while becoming an open wave (Fig. 4b). There appears to be a broad area of diffluence across the Central and Northern Plains, but this is not as apparent at 300 hPa. The short-wave trough in the Dakotas had lifted into southern Canada, while the other disturbance had moved into western Kansas and Nebraska. Despite the eastward movement of the upper-level closed low and observed height falls across the Western High Plains, slight warming was observed at 500 hPa from Rapid City, South Dakota (RAP) to Dodge City, Kansas (DDC). Cold air advection (CAA) was indicated though at 700 hPa across this same area, as the thermal ridge had shifted eastward during the day. The moisture axis at 850 hPa remained stationary through the day, with some retrogression noted across western areas of Nebraska and Kansas (Fig. 4d). The nocturnal low-level wind maxima present at 1200 UTC weakened, and backing of the wind flow is apparent across the Great Plains states.

b. Surface analysis

A complicated surface pattern existed across the Central Plains at 1200 UTC 5 June (Fig 5). Surface lows were analyzed in eastern South Dakota and west-central Nebraska. The primary synoptic feature at this time was a front that extended from western Minnesota into southern South Dakota. A double dryline structure was analyzed at 1200 UTC. The eastern dryline extended from eastern Nebraska into western Kansas, which had advanced eastward from 0000 UTC 5 June until 1200 UTC 5 June due to the passage of a previous short-wave. A second dryline extended across eastern Colorado. The greatest low-level moisture was confined to areas south and east of the eastern dryline, with dewpoints of 12 to 15 °C noted behind the boundary and 18 to 21 °C ahead of it.

Figure 6 depicts 3-hourly subjective surface analyses from 1500 UTC 5 June through 0000 UTC 6 June. As the day progressed, low pressure over western Nebraska deepened due to the approach of the main upper-level system (Fig. 6 b-d). This resulted in backing of the low-level winds and an increase in moisture across western Nebraska and Kansas.Strengthening and backing of the low-level flow also led to an increase in surface moisture convergence along the various surface boundaries. Figure 7 depicts the change in moisture convergence associated with the northward movement of low-level moisture. This is also the general area where convection first developed near 1800 UTC. By 2100 UTC and 0000 UTC (Fig. 7c and d), surface moisture convergence significantly increased along both the stationary front across northern Nebraska and southern South Dakota, as well as the dryline that extended north to south across western Nebraska.

c. Convective parameters

An analysis of common environmental convective parameters showed that conditions appeared favorable for a regional tornado outbreak. Due to the presence of steep mid-level lapse rates and significant low-level moisture, the atmosphere was unstable across the Central Plains. As the boundary layer mixed and deepened through the afternoon, 100 hPa mixed layer convective potential energy (MLCAPE) increased across the area (Fig. 8). The effect of the increase in stability from the passage of the surface trough prior to 1200 UTC was apparent at North Platte, Nebraska (LBF), with the atmosphere comparatively stable at 1200 and 1800 UTC. Due to the rapid boundary layer moisture return during the afternoon, the 0000 UTC 6 June sounding at LBF showed rapid destabilization. Deep-layer shear also appeared favorable for supercells across the risk area through the day, with 0 to 6 km cumulative shear above 20 m s^{-1} which has been shown to be favorable for supercells and tornadic supercells (Rasmussen and Blanchard 1998) (Fig. 9). The 0 to 1 km shear (Fig. 10) was enhanced at 1200 UTC 5 June due to the effects of the nocturnal low-level jet. With the weakening of the nocturnal jet, the 0 to 1 km shear dropped by 1800 UTC, but as the upper-level short-wave approached by 0000 UTC 6 June, values once again increased to approximately 10 m s^{-1}, which has been shown to support tornadic supercells (Thompson et al. 2002). Using observed supercell storm motion, and the observed 0000 UTC 6 June hodograph from LBF (Figure 11), the vertical wind profile was similar to what Bunkers (2000) found supportive of tornadic supercells with high values of storm relative helicity and cumulative shear. This atmosphere was also well anticipated by operational forecasters, as the 1300 UTC severe weather outlook for day 1 (SWODY1) from the Storm Prediction Center indicated:

"Vertical Shear is expected to be quite favorable for supercells

and potentially significant tornadoes...with SRH (storm relative helicity) 300-500 J/KG...BRN (Bulk Richardson number) shears of 70-120 J/KG...and SR (storm relative) flow generally AOA (at or above) 20 kt through most of the troposphere."

Although the decrease in boundary layer moisture across the risk area with the passage of the surface dryline prior to 1200 UTC led to a decrease in surface parcel buoyancy, it does not appear that this was sufficient to decrease the risk of significant tornadic supercells. The return of low-level moisture through the afternoon was apparent in the surface analysis presented in Figure 6. Dewpoints across the risk increased into the 13 °C to 18 °C range by 0000 UTC 6 June. The increase in boundary layer moisture is apparent in the series of observed soundings from LBF (section 4d). This increase in low-level moisture was also apparent when the lifted condensation level (LCL) on the 1200 and 1800 UTC 5 June LBF observed sounding is compared to the 0000 UTC 6 June observed sounding (not shown). The LCL increased from 545 m on the 1200 UTC sounding to 1630 m on the 1800 UTC sounding. As the low-level moisture advected into the region, the LCL on the 0000 UTC 6 June sounding decreased to 1267 m. This LCL height is slightly above the range of 500 m to 1100 m found by Rasmussen and Blanchard (1998) to be most supportive of tornadic supercells[2].

4. Identification of the Inhibiting Factors

It is hypothesized that the inhibiting factor that appears to have prevented the significant tornado outbreak on 5 June 1999 was the presence of persistent mid-level subsidence. The

[2] Later research by Rasmussen (2003) indicated their findings in 1998 may have more utility in forecasting supercells with large hail than differentiating between tornadic and non-tornadic supercells.

presence of the mid-level subsidence is identified using a time series of relative vorticity, heights, and isotachs at the 500 hPa level. This hypothesis will be supported by examination of analyses fields of the RUC model and satellite data. Soundings will also be provided to explain the role of moisture advection on the convective environment and to identify the presence of the subsidence.

a. 500 hPa Analysis

Examination of the 500 hPa analyses of relative vorticity, heights, and isotachs during the event shows a number of short-wave disturbances in the vicinity of the main upper trough over the Great Basin. These short-wave features are labeled #1 through #5 in Figure 12. This study will concentrate on the movement and location of short-waves #3 and #4. At 0000 UTC 5 June, short-wave #3 was over the western Texas panhandle, and short-wave #4 was located in the base of the trough over western Arizona. By 1200 UTC 5 June, short-wave #3 had ejected into the Northern Plains, while short-wave #4 had moved into New Mexico (Fig. 12b). By 0000 UTC 6 June 1999, short-wave #3 had moved into the upper Mississippi Valley with short-wave #4 into the central High Plains (Fig. 12c). A short-wave ridge is apparent between short-wave #3 and #4 which moved directly over the risk area during peak heating.

A cross-section at 1200 UTC 5 June of vertical motion (ω) from Hill City, KS, (HLC) to Valentine, NE, (VTN) showed that the overall atmospheric motion from HLC across western Nebraska was characterized by subsidence (Fig. 13a). Closer to VTN in northern Nebraska, there is upward vertical motion up to near 500 hPa, with little motion noted above that level. This large-scale subsidence in the cross-section appears to correspond well to the shortwave ridge identified in Figure 12. By 0000 UTC 6 June (Fig. 13b) stronger vertical motion had over-spread

most of central and northern Nebraska associated with shortwave #4. Farther south along the dryline into northwest Kansas, subsidence continues to be observed.

b. RUC analyses

The model analysis fields of the RUC NCEP model from 1200 and 1800 5 June and 0000 UTC 6 June model were used to produce an analysis of the 200 to 400 hPa Q-vector field and the 400 to 700 hPa Q-vector field (Fig. 14). These upper-level Q-vector analyses were used to resolve the large-scale vertical motion. At 1200 UTC 5 June, forcing for large-scale subsidence can be seen at both 200 to 400 hPa and 400 to 700 hPa across all of the risk area (Figs. 14a and b). This continued through 1800 UTC (Figs. 14c and d). These analyses support the notion that despite good solar insolation and boundary layer mixing, forcing for large-scale subsidence across the risk area from 1200 UTC until 1800 UTC 5 June likely inhibited large-scale upward vertical motion. The lack of forcing for large-scale ascent continued through the afternoon over a large part of the risk area (Figs. 14e and f). Only areas of far western Nebraska into southwest South Dakota indicate forcing for large-scale ascent by 0000 UTC 6 June.

c. Role of moisture advection

Although not a direct negative factor, moisture advection appears to have led to the development of thunderstorms over parts of the risk area prior to peak heating. The presence of clouds associated with this moisture advection likely inhibited some of the surface heating across the eastern high risk area.

High Θ_e air had been displaced to the south across Kansas and Oklahoma by 1200 UTC 5 June with the passage of short-wave #3. With the approach of short-wave #4, the moist air pushed rapidly northward during the late morning and early afternoon. This moisture advection,

centered near 800 hPa, is identifiable in a cross-section from Dodge City, KS, to Sioux City, IA (Fig. 15). Moisture advection during the late morning and early afternoon is also suggested in the visible satellite imagery as an area of mid-level clouds over the Kansas at 1500 UTC (Fig. 16a), which then moved northeast into Nebraska by 1800 UTC (Fig. 16b and c). Convection developed at the nose of this region of moisture advection, over northeast Nebraska, and pushed into southern Minnesota by 2100 UTC (Fig. 16d). This convection was responsible for many of the severe weather reports over northeast Nebraska, southeast South Dakota, northern Iowa, and southern Minnesota (Fig. 2).

d. Sounding analyses

Due to the anticipated convective outbreak, special 1800 UTC soundings were taken at locations within the risk area to provide additional information on the evolution of the convective environment. The existence of moisture advection is most visible at OAX with the increase in relative humidity from 850 to 700 hPa (Fig. 17). By 0000 UTC 6 June, the inversion near 800 hPa had been eroded, but a new inversion had developed between 700 and 600 hPa. Evidence of moisture increase near the inversion, with significant drying noted just above, indicates this may be a subsidence inversion and not the elevated mixed layer (AWS/TR-79/006) as in the 1200 and 1800 UTC soundings. The effect of the moisture advection is less defined in the Topeka, KS (TOP) sounding, although there is a slight increase in temperature from 1200 to 0000 UTC in the EML which suggests a lack of cooling in this layer (Figs. 18). When the OAX and TOP soundings are compared through the period, the height and structure of the inversions appear different, which supports the hypothesis that the OAX inversion is a subsidence inversion and not EML. Like the OAX soundings, there is a strong moisture advection signal in the LBF

soundings from 1200 through 0000 UTC. Despite strong moisture advection, large-scale ascent associated with short-wave #4 from 1800 UTC through 0000 UTC 6 June allowed for slight cooling of the mid-levels, after slight warming from 1200 UTC to 1800 UTC (Fig. 19).

Boundary layer mixing is most visible on the OAX and TOP soundings, with an increase in the level of free convection (LFC) from 1200 UTC to 0000 UTC 6 June. Despite the boundary layer turbulent mixing and moisture advection, the TOP and OAX soundings remained capped at 0000 UTC. The convective inhibition at LBF was nearly eroded by 0000 UTC, which allowed for an area of convective initiation across western Nebraska. The absence of CIN across parts of western Nebraska also supports the hypothesis of mid-level subsidence over a large part of the risk area as a negative factor since both the OAX and LBF soundings indicate moisture advection from 1200 through 0000 UTC, but the OAX sounding remains capped.

e. Satellite analysis

The role of large-scale subsidence that appeared to negate widespread convective initiation on 5 June, is also evident in satellite data. The 3-hourly water vapor (6.7 μm) imagery from 1515 UTC 5 June through 0015 UTC 6 June is presented in Figure 20. The two main features evident are the upper-level cyclone over the central Rocky Mountains and the anticyclonically curved moisture feed extending from the Texas panhandle into central Nebraska which represents the subtropical jet (Fig. 20a). By 1815 UTC 5 June, the subtropical jet extended into Nebraska and northern Iowa (Fig. 20b), and the western edge of this feature remained nearly stationary through 2115 UTC (Fig. 20c). To the west of the subtropical jet an anticyclonically curved darkening is apparent in the water vapor imagery between short-wave #3 (over the Upper Mississippi River Valley) and short-wave #4 (over eastern Colorado) suggesting that a lack of

forcing for large-scale vertical motion was taking place above the boundary layer as indicated in the soundings from OMA and TOP. The anticyclonically curved darkening is similar to one described in the RB03 study. The hypothesis that this darkening on water vapor imagery can be related to subsidence was also suggested by Weldom and Holmes (1991).

In addition to the water vapor imagery, visible satellite imagery indicated widespread surfaced-based towering cumulus (TCU) developed across Nebraska and South Dakota between 2100 UTC and 0000 UTC (Fig. 21). Field observations from one of the authors this day, however, indicate that parcels ceased to be buoyant once their updrafts reached the base of the subsidence inversion. Numerous towers were observed that quickly spread into an altocumulus sheet. This supports the idea suggested by the satellite data that mid-level subsidence occurred in the wake of short-wave #3. This subsidence appears to have helped to maintain a capping inversion that prevented surface-based convection over most of the severe threat area. The only area where sustained convection was able to develop was over far northwest Nebraska (Fig 21b), where little convective inhibition remained. The convective activity here was responsible for the severe storm reports over north central Nebraska and extreme southern South Dakota (Fig. 2).

5. Forecasting the event

The main factor that likely precluded a significant tornado outbreak was the lack of large-scale support for vertical motion between short-wave #3 and #4. An important operational consideration is to determine if this factor could have been forecast. As discussed in Johns and Doswell (1992), four basic ingredients are needed for severe storms: sufficient moisture, instability, and lift for parcels to reach the LFC, and strong vertical wind shear. It has been

shown that on 5 June that sufficient moisture, instability, and favorable vertical shear were present for severe storms, and the degree of instability and shear suggested that significant tornadic supercells were possible. Sufficient lift for parcels to reach the LFC appeared to be the lacking ingredient.

When the model analysis fields of the NCEP RUC (Fig. 14) model are compared to 1200 UTC 5 June runs of the ETA, AVN, and NGM (operational models), general agreement in the large-scale pattern is apparent (output fields from the ETA, AVN, and NGM are not shown as they were similar to those of the RUC). All three models depicted Q-vector convergence initialization fields similar to those of the RUC. By 1800 UTC 5 June, the 6-hour forecasts from the operational models continued to forecast Q-vector divergence between short-waves #3 and #4 across the risk area. Although the operational models identified forcing for large-scale subsidence above 600 hPa, the operational numerical forecast model soundings indicated cooling taking place within the EML around 700 hPa. In figure 22, the Eta 6-hour forecast soundings for LBF, Minneapolis, MN (MPX), OAX, and TOP are compared to the observed soundings at 1800 UTC (the Eta was used due to its finer vertical resolution). The largest difference was at OAX (Fig. 22c) where strong erosion of the elevated mixed layer was forecast to occur. The same forecast error could also be seen at LBF, MPX, and TOP, where the EML inversion (800 to 650 hPa) remained stronger than forecast (Figs. 20 b, c, and d respectively). The model error led to a significant forecast error in the amount of convective inhibition (CIN) by 1800 UTC 5 June.

By 0000 UTC 6 June, the operational models remained in general agreement concerning large-scale forcing for vertical motion. The models forecast that forcing for ascent would move into western Nebraska, with forcing for large-scale subsidence forecast across most of the risk

area. Despite the agreement in the upper-level synoptic scale forcing pattern, the 12 h forecast soundings valid 0000 UTC 6 June from the Eta continued to show significant errors in the degree of CIN remaining across the Plains. Although the boundary layer deepened through the afternoon, 50 to 90 J kg^{-1} of CIN remained in the observed soundings OAX and TOP, whereas the forecast soundings erroneously indicated that only about 10 J kg^{-1} of CIN remained (Fig. 23). The model forecast soundings and the observed soundings at 0000 UTC 6 June matched most closely at LBF, where the forecast and observed temperature profiles were nearly identical, and a well-mixed boundary layer with steep mid-level lapse rates was indicated (Fig. 23a) .

On 5 June 1999 all three of the operational models produced precipitation across the eastern half of the risk area between 1800 to 0000 UTC. The development of model derived precipitation across part of the risk area led to significant differences in model convective profile and what was taking place in reality. Baldwin and Kain (2002) identified two cases where the Betts-Miller-Janjic (BMJ) convective parameterization and, in particular, its shallow convective scheme (Betts 1986; Betts and Miller 1986; Janjic 1994) led to model forecast errors of the thermodynamic profile of the lower troposphere. Although it is possible the shallow convective scheme of the Eta contributed to the forecast error within its inversion layer, this is not likely the primary reason for the forecast error since the AVN and NGM do not use the BMJ convective scheme.

We hypothesize that in the case of 5 June 1999 the models correctly forecast the vertical motion associated with moisture advection. Lift associated with the moisture advection appeared to moisten and cool the inversion layer in all operational models which led to a production of precipitation. In reality the moisture advection resulted in convective initiation over northeast

Nebraska and Iowa during the early afternoon hours, but the presence of the shortwave ridge upstream of this convection was not well represented in model forecast soundings due to the development of convection within the model. The production of convection within the model allowed for a redistribution of heat, changes in vertical stability, and a redistribution of moisture. These changes within the model did not allow for sufficient representation of the developing subsidence inversion across parts of the risk area.

The degree of error can be seen when the 700 hPa temperatures from the 1200 UTC 5 June Eta model analysis, 6 hour forecast, and 12 hour forecast fields are compared to the observed 700 hPa temperature field (Fig. 24). The 1200 UTC initialization showed good agreement with observations across the Central Plains, with a 1°C error at MPX, likely due to ongoing convection, and a 2°C error at Denver, Colorado (DEN) (Fig. 24a). By 1800 UTC, the Eta forecast had cooled the 700 hPa temperatures across the Central Plains, but the observed 1800 UTC soundings indicate that temperatures remained steady at around +12°C (Fig. 24b). The Eta model was too progressive in advecting colder air associated with the Rockies upper-level cyclone east into the western High Plains, with a 1°C error at DEN and a 3°C error at Rapid City, SD (RAP). There also were significant differences at OAX, with a 4°C error, and at TOP with a 3°C error. By 0000 UTC, observed 700 hPa temperatures had cooled slightly over western Kansas, Nebraska, and South Dakota, as was rather well forecast by the models (Fig 24c). The observed 700 hPa temperatures continued to be warmer than forecast however from eastern Kansas northeast into Minnesota, with a 3°C error in TOP and 2°C error observed at both Springfield, MO (SGF) and MPX.

When comparing the model forecasted fields to the observed data for 5 June 1999, it appears that while the models correctly forecast the degree and location upper-level synoptic scale forcing with reasonable accuracy, significant errors existed in the model forecast soundings. Differences in the thermodynamic profiles of the atmosphere led to significant differences in the amount of CIN forecast to be present during the afternoon hours of 5 June. The differences between model forecasts and observations illustrate the importance in comparing observational and model data to identify possible errors that could facilitate diagnosing inhibiting factors.

6. Conclusion

On 5 June 1999 a significant tornado outbreak was forecast across parts of the Central and Northern Plains. This study looks at 5 June in order to determine why a limited, rather than major, tornado outbreak occurred. Using conceptual models developed for severe weather forecasting, it has been shown that ample instability, moisture, and vertical wind shear were indeed present for a significant tornado outbreak. Across a large part of the risk area, however, synoptic-scale lift was too weak to reduce the capping inversion and create an environment favorable for surface parcels to reach the LFC. The primary limiting factor appears to have been a migratory short-wave ridge over the risk area during peak heating. This synoptic-scale forcing for large-scale subsidence was visible in water vapor imagery, observational soundings, and forecast analysis of the RUC model. Subsidence above the EML seemed to have limited the aerial extent of the severe weather on 5 June. Where severe weather did develop, some

significant, mesoscale influences appear to have overcome the synoptic-scale forcing for subsidence.

Subjective forecasting of the inhibiting factors on 5 June appears possible with help of observation data and synoptic scale forecast guidance of numerical models. The main numerical model forecast error appears to have developed within the inversion layer due to the development of precipitation during the afternoon. The production of precipitation seems to have allowed for alterations in the thermodynamic profile and a reduction in the amount of forecast CIN. This subsequently increases the threat of convective initiation despite the synoptic-scale forcing for subsidence. When utilizing the observed data and RUC analyses, and comparing this data to the operational Eta, AVN, and NGM, few significant differences were noted in the upper-level synoptic-scale forcing patterns. All of the operational forecast models indicated forcing for large-scale subsidence across the risk area through the day on 5 June. Observational data indicated a lack of forcing for large-scale vertical ascent between short-wave trough #3 and #4, which counteracted diurnal weakening of the CIN. Only in areas of western Nebraska and southwest South Dakota did large-scale forcing for ascent occur; this forcing, coupled with turbulent boundary layer mixing and CAA in the mid-levels from short-wave #4, allowed surface-based convective initiation to occur. Across the rest of the risk area, model forecast temperatures at 700 hPa were cooler by at least 2 ºC compared to observational data.

Operational forecasters are strongly encouraged not to use models to asses the convective environment when the models have produced convection prior to the time of diagnosis. As seen in the case of 5 June 1999, using models that have initiated their convective scheme and

produced precipitation to forecast the environment can lead to significant errors in the thermal and moisture profiles, and lead to errors in forecast CAPE and CIN.

We have defined a null event as a non-occurrence of any forecast weather element. As indicated from other published research on null events, including D02 and RB02, the inhibiting factor may occur on the synoptic-scale or the mesoscale. It also appears that a synoptic scale inhibiting factor can either limit the amount of severe weather, as in the case presented here on 5 June, or eliminate the threat of severe weather as in RB02 study. Although it has been shown that the forcing for convective initiation occurs on the mesoscale, as in the D87 study, the mesoscale forcing can overcome a synoptic environment which does not support widespread convective initiation, or as in the D02 study, inhibit the expected type of severe weather. It appears that widespread significant severe weather is most likely when both the synoptic and mesoscale support significant severe weather.

In addition to the identification of a synoptic-scale inhibiting factor that led to a reduced risk of significant tornadoes, for operational forecasters, there were clues in both the observed data as well as model data prior to the event that could have provided valuable lead time to forecast users and can be applied to future severe weather situations. Potential inhibiting factors should closely be monitored through the use of detailed subjective analyses, analyses of observed data, and careful examination of numerical model data. It is possible that certain inhibiting factors, such as a short-wave ridge or a local mesoscale effect, are more common to specific regions; local awareness of mesoscale effects can lead to better convective forecasts.

7. References

Anthony, A. W., P. W. Leftwich Jr., 1992: Trends in severe local storm watch verification at the National Severe Storms Forecast Center. *Wea. Forecasting*, **7**, 613-622.

Baldwin, M.E., and J. S. Kain, 2002: Properties of the convective scheme in NCEP's Eta model that affect forecast soundings interpretation. *Wea. Forecasting*, **17**, 1063-1078.

Barnes, S. L., F. Caracena, and A. Marroquin, 1996: Extracting synoptic-scale diagnostic information from mesoscale models: The Eta model, gravity waves, and quasigeostrophic diagnostics. *Bull. Amer. Meteor. Soc*., **77**, 519-528.

Benjamin, Stanley G., G. A. Grell, J. M. Brown, T. G. Smirnova, R. Bleck, 2004: Mesoscale weather prediction with the RUC hybrid isentropic terrain-following coordinate model. *Mon. Wea. Rev*., **132**, 473-494.

Betts, A. K., 1986: A new convective adjustment scheme. Part I: Observational and theoretical basis. *Quart. J. Roy. Meteor. Soc*., **112**, 677-691.

_____, and M. Miller, 1986: A new convective adjustment scheme. Part II: Single column test using GATE wave, BOMEX and arctic air-mass data set. *Quart. J. Roy. Meteor. Soc*., **112**, 693-709.

Bunkers, M. J., B. A. Klimowski, J. W. Zeitler, R. L. Thompson, M. L. Weisman, 2000: Predicting supercell motion using a new hodograph technique. *Wea Forecasting*, **15**. 61-79.

Concannon, P. R., H. E. Brooks, and C. A. Doswell III, 2000: Climatological risk of strong and violent tornadoes in the United States. Preprints, *Second Conf. on Environmental Applications,* Long Beach, CA. Amer. Meteor. Soc., 9.4.

DesJardins, M. L., K. F. Brill, and S. S. Schotz, 1991: GEMPAK5 user's guide. NASA Technical Memorandum, 4260 pp. [available from NASA, Code NTT-4, Washington, DC 20546-0001.]

Doswell, C. A., III, 1987: The distinction between large-scale and mesoscale contribution to severe convection: A case study example. *Wea. Forecasting*, **2**, 3-16.

_____, D. V. Baker, and C. A. Liles, 2002: Recognition of negative mesoscale factors for severe-weather potential: A case study. *Wea. Forecasting*, **17**, 937-954.

Edwards, R., S. F. Corfidi, R. L. Thompson, J. S. Evans, J. P. Craven, J. P. Racy, D. W. McCarthy, and M. D. Vescio, 2001: Storm Prediction Center forecasting issues Related to the 3 May 1999 tornado outbreak. *Wea. Forecasting*, **17**, 544-588.

Fujita, T. T., 1981: Tornadoes and downbursts in the contest of generalized planetary scales. *J. Atmos. Sci*., **38**, 1511-1534.

Hart, J. A., and W. Korotky, 1991: The SHARP workstation v1.50 users guide. National Weather Service, NOAA, US. Dept. of Commerce, 30 pp.

Janjic, Z. I., 1994: The step-mountain eta coordinate model: Further developments of the convection, viscous sublayer, and turbulence closure schemes. *Mon. Wea. Rev*., **122**, 927-945.

Johns, R. H., and C.A. Doswell III, 1992: Severe local storms forecasting. *Wea. Forecasting*, **7**, 588-612.

McNulty, R. P., 1995: Severe and convective weather: A central region forecasting challenge. *Wea. Forecasting*, **10**, 187-201.

NCDC, 1999: *Storm Data*. Vol. 45, No. 6, 386 pp. [Avaliable from National Climate Data Center, 151 Patton Ave., Ashville, NC 28801-5001.]

Rasmussen, E. N., 2003: Refined supercell and tornado forecast parameters. *Wea. Forecasting*, **18**, 530-535.

_____, and D. O. Blanchard, 1998: A baseline climatology of sounding-derived supercell and tornado forecast parameters. *Wea. Forecasting*, **13**, 1148-1164.

Richter, H., and L. Bosart, 2002: The suppression of deep moist convection near the Southern Great Plains dryline. *Mon. Wea. Rev.*, **130**, 1665-1691.

Rogers, E., T. L. Black, D. G. Deaven, G. J. DiMego, Q. Zhao, M. Baldwin, N. W. Junker, and Y. Lin, 1996: Changes to the operational "early" Eta analysis/forecast system at the National Centers for Environmental Prediction. *Wea. Forecasting*, **11**, 391-416.

Stensrud, D. J, R. A. Maddox, 1988: Opposing mesoscale circulations: A case study. *Wea. Forecasting*, **3**, 189-204.

Thompson, R. L., R. Edwards, and J. A. Hart, 2002: Evaluation and interpretation of the

supercell composite and significant tornado parameters at the storm prediction center. Preprints, *21st Conf. on Severe Local Storms.* San Antonio, TX,. Amer. Meteor. Soc., J11.

Thompson, R.L. and R. Edwards, 2000: A comparison of rapid update cycle 2 (RUC-2) model soundings with observed soundings in supercell environments. Preprints, *20th Conf. Severe Local Storms*, Orlando, FL.

Weldon, R. B., and S. J. Holmes, 1991: Water vapor imagery interpretation and applications to weather analysis and forecasting. NOAA Technical Report NESDIS 57, 85.

8. Figures

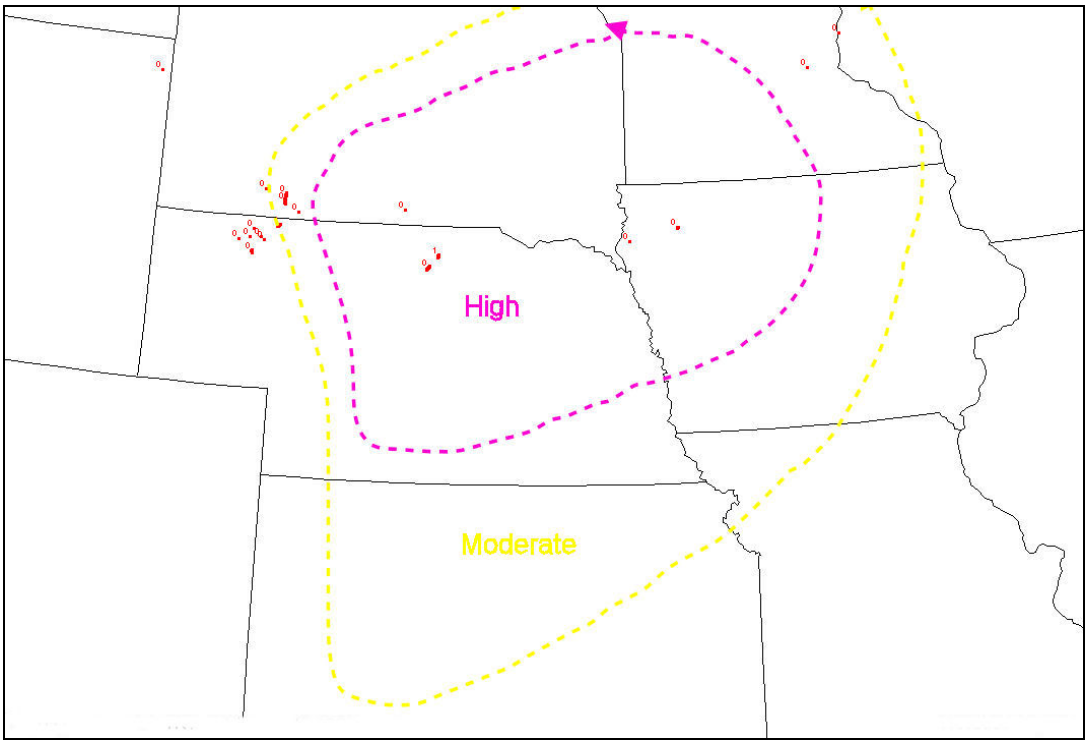

Figure 1. The 1630 UTC NOAA/NWS/NCEP Storm Prediction Center convective outlook valid 1630 UTC 5 June 1999 through 120 UTC 6 June 1999. Tornado reports from 1200 UTC 5 June through 0600 UTC 6 June are plotted in red along with their corresponding strengths. Tornado reports are from Storm Data.

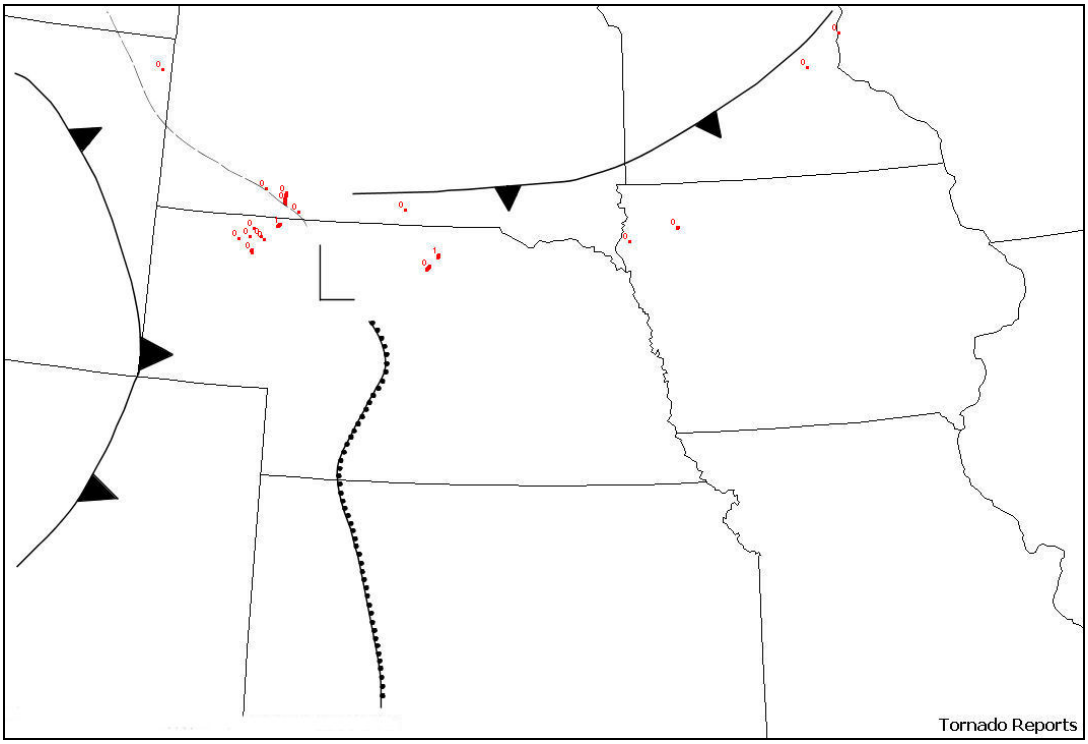

Figure 2. Same as figure 1, but with the 2100 UTC 5 June subjective surface fronts overlaid.

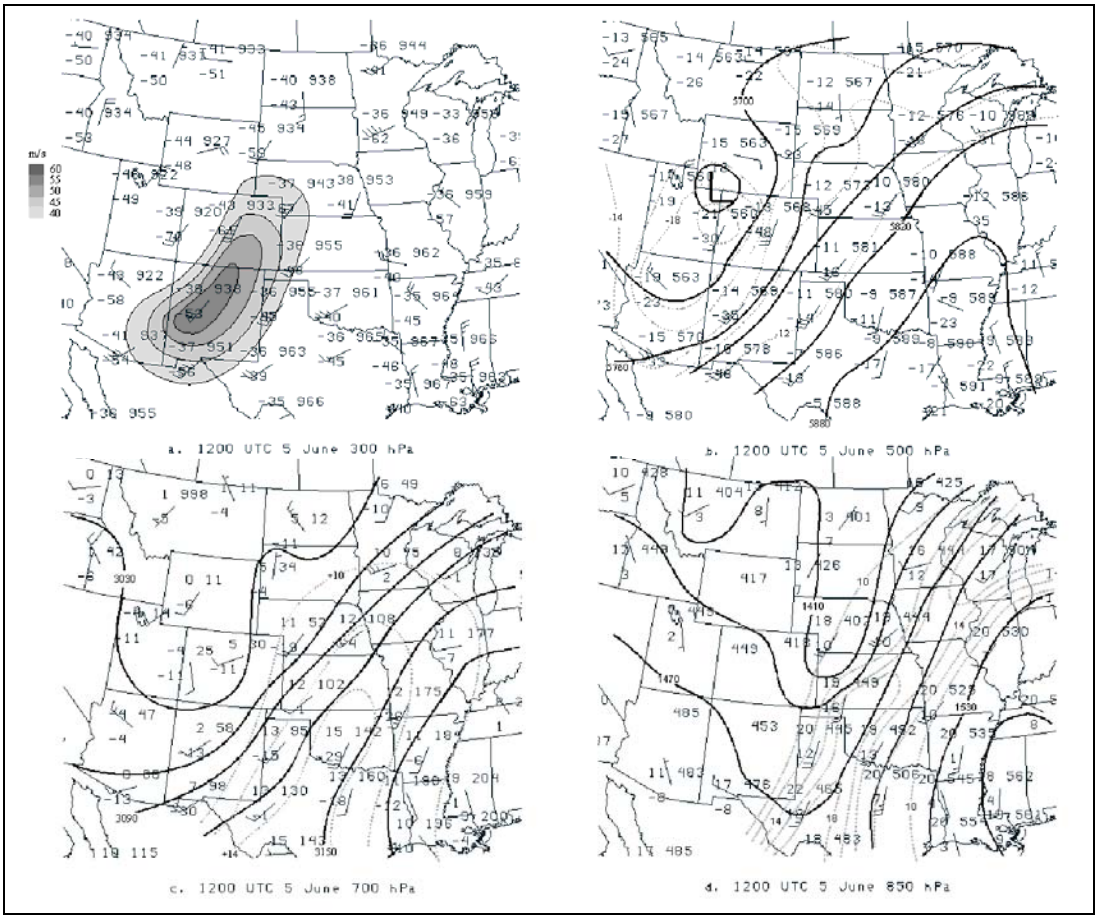

Figure 3. 1200 UTC 5 June subjective upper air analyses. (a) is 300 hPa jet stream analysis. Isotach are contoured ever 5 ms^{-1} from 40 to 60 ms^{-1}. (b) is the 500 hPa analysis. Heights (solid lines) are contoured every 60 m. Temperatures, light dashed lines, are contoured every 2 °C and labeled every 4 °C from -20 °C to -10 °C. (c) is the 700 hPa. Heights (solid lines) are contoured every 30 m, and labeled every 60 m. Temperatures, light dashed lines, are contoured every 2 °C starting at +10 °C . (d) is the 850 hPa analysis. Heights (solid lines) are contoured every 30 m, and labeled every 60 m. Dewpoints (light dashed lines) are contoured every 2 °C starting at +10 °C. Wind is in m s^{-1} for all times (long barb = 5 m s^{-1}, short barb = 2.5 m s^{-1}).

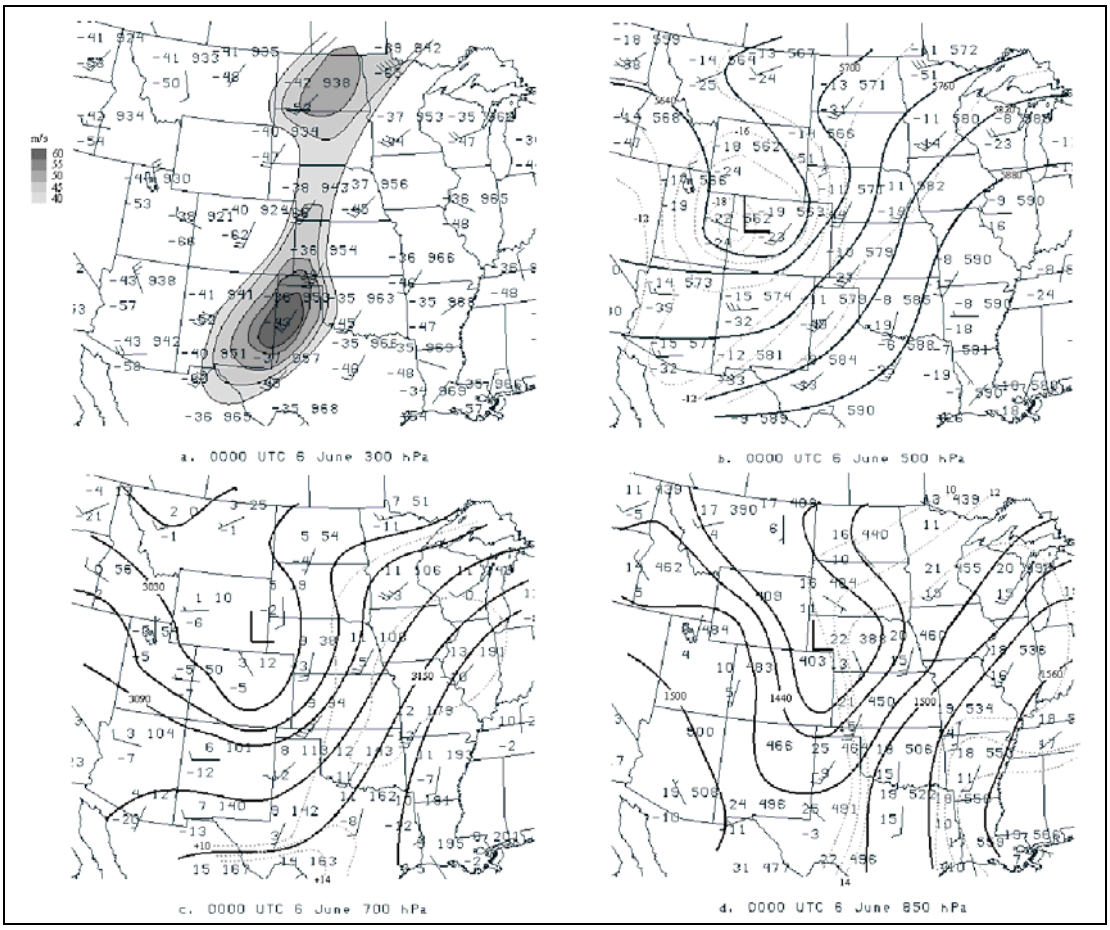

Figure 4. Same as figure 3, for 0000 UTC 6 June.

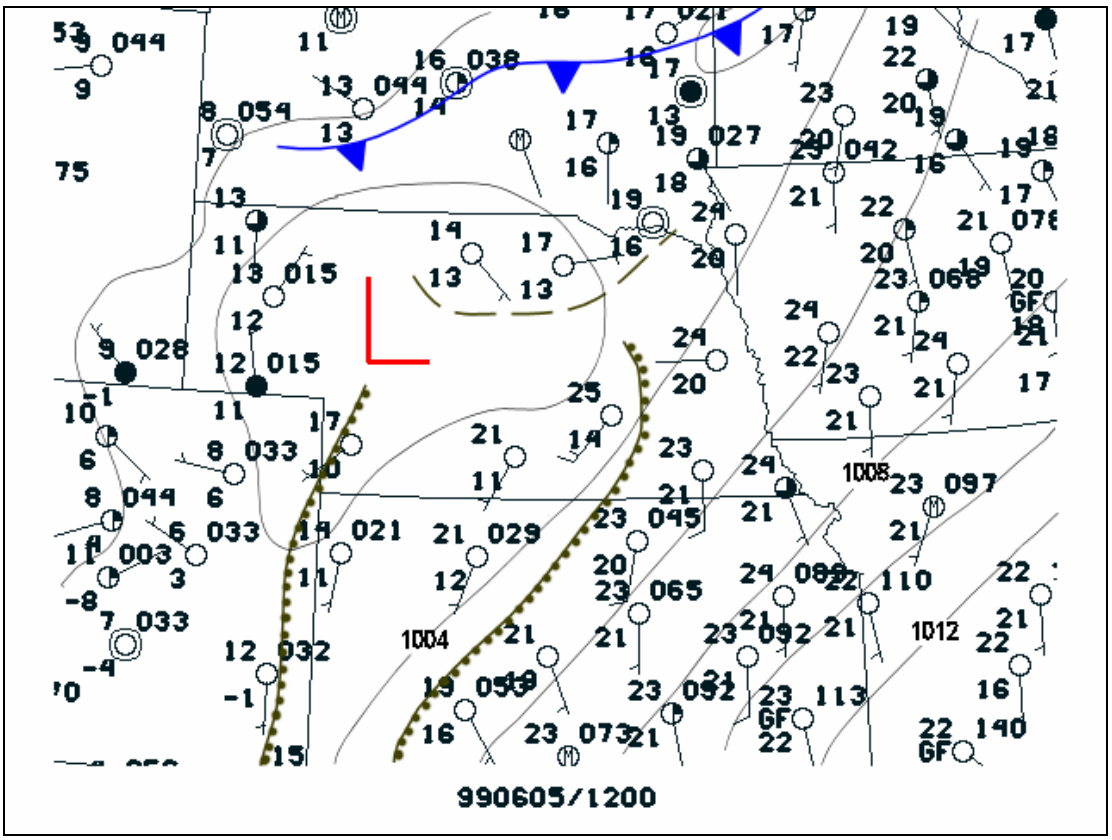

Figure 5. Objective surface pressure analysis for 1200 UTC 5 June 1999. Pressure is in hPa, temperature and dewpoint are in EC. Wind is shown in m s^{-1} (long barb = 5 m s^{-1}, short barb = 2.5 m s^{-1}).
Dashed brown line indicates location of surface outflow boundary.

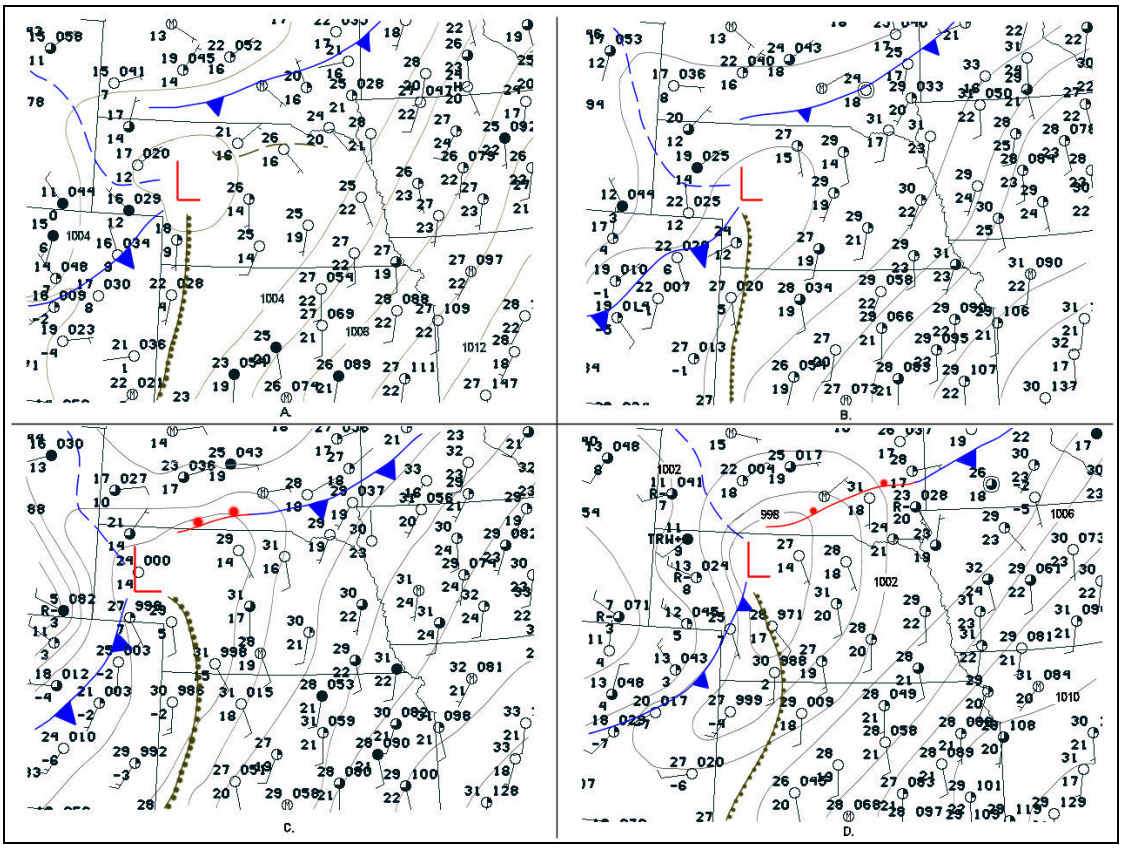

Figure 6. Subjective surface analyses for 1500 UTC (a), 1800 UTC (b), 2100 UTC 5 June (c), and 0000 UTC 6 June (d). Pressure is in hPa, temperature and dewpoint are in EC. Wind is shown in m s^{-1} (long barb = 5 m s^{-1}, short barb = 2.5 m s^{-1}). Dashed lines indicate location of surface troughs.

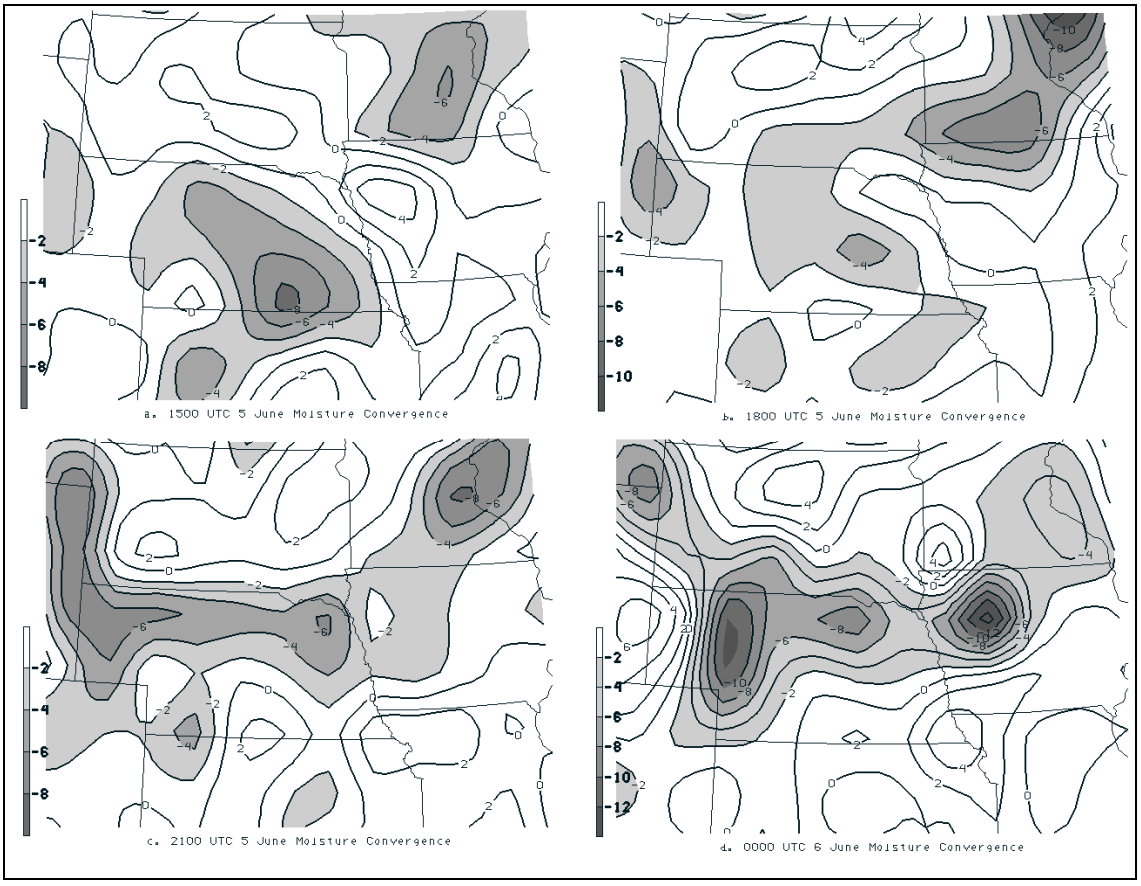

Figure 7. Objective surface moisture divergence from 1500 UTC (a), 1800 UTC (b), 2100 UTC (c), and 0000 UTC (d). Shaded areas indicate surface moisture convergence. Units are s^{-1}.

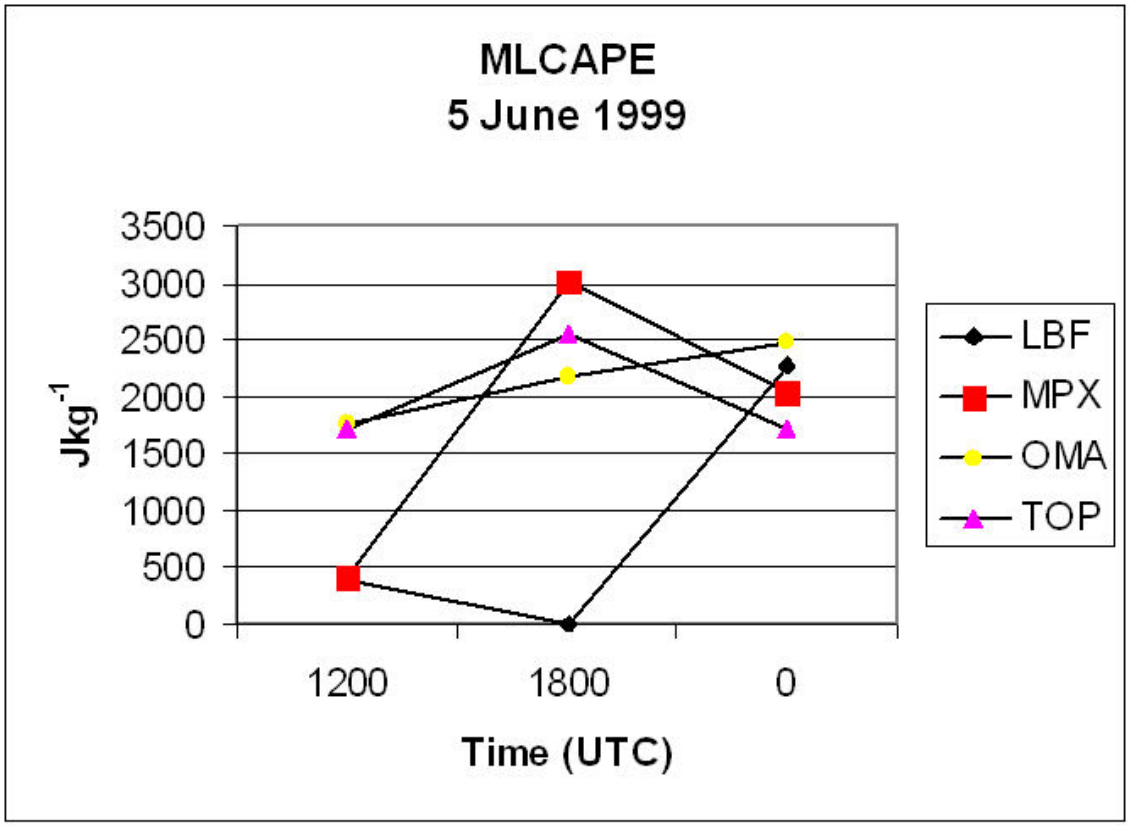

Figure 8. Line graph of the 100 hPa mixed layer CAPE (MLCAPE) from 1200 UTC 5 June through 0000 UTC 6 June, for the locations of North Platte, NE (LBF), Minneapolis, MN (MPX), Omaha, NE (OAX), and Topeka, KS (TOP). Y-axis is MLCAPE in j kg^{-1}, and the X-axis is time in UTC.

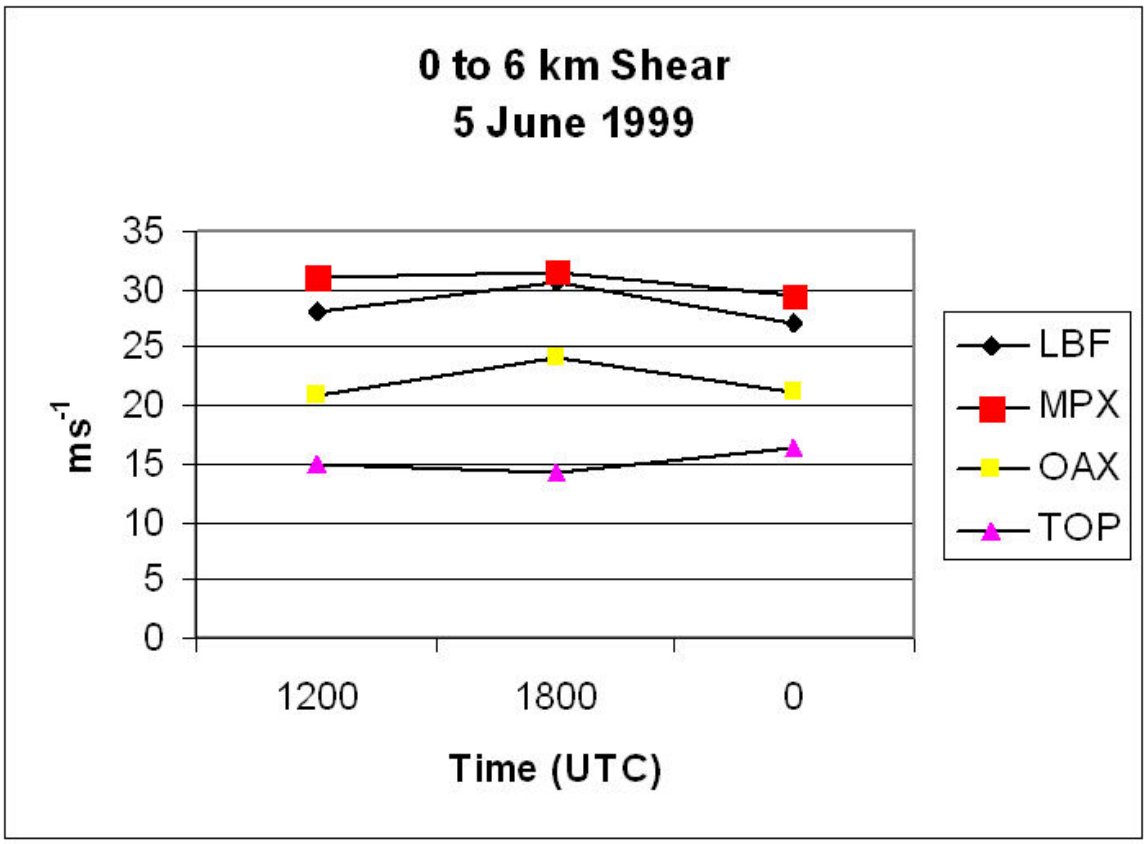

Figure 9. Line graph of the 0 to 6 km cumulative shear for 1200 UTC 5 June through 0000 UTC 6 June. Same locations as in Fig. 6. Y-axis is in m s^{-1}, and the X-axis is time in UTC.

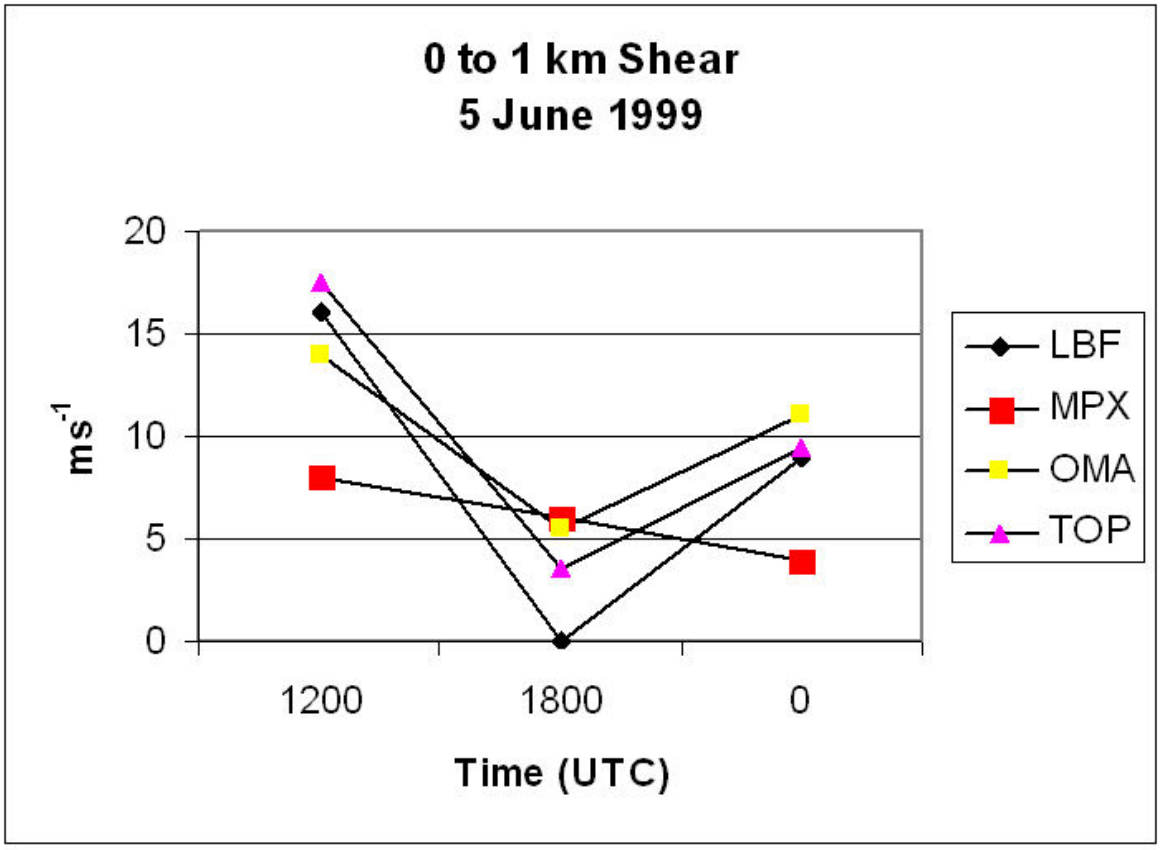

Figure 10. Same as Fig. 7 for 0 to 1 km.

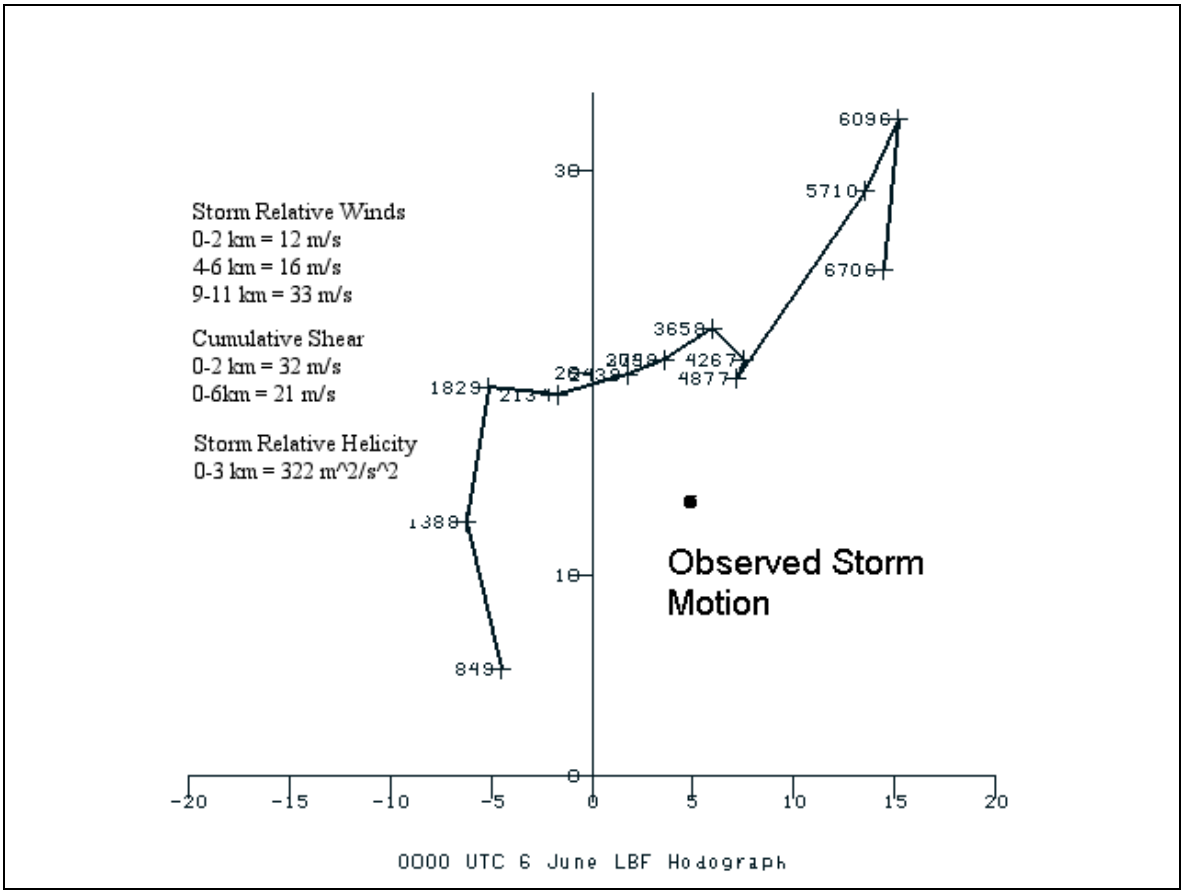

Figure 11. Observed 0000 UTC 6 June hodograph from North Platte, NE. Wind components (u and v) are in m s^{-1}, and heights are in meters. Environmental calculations used observed storm motion.

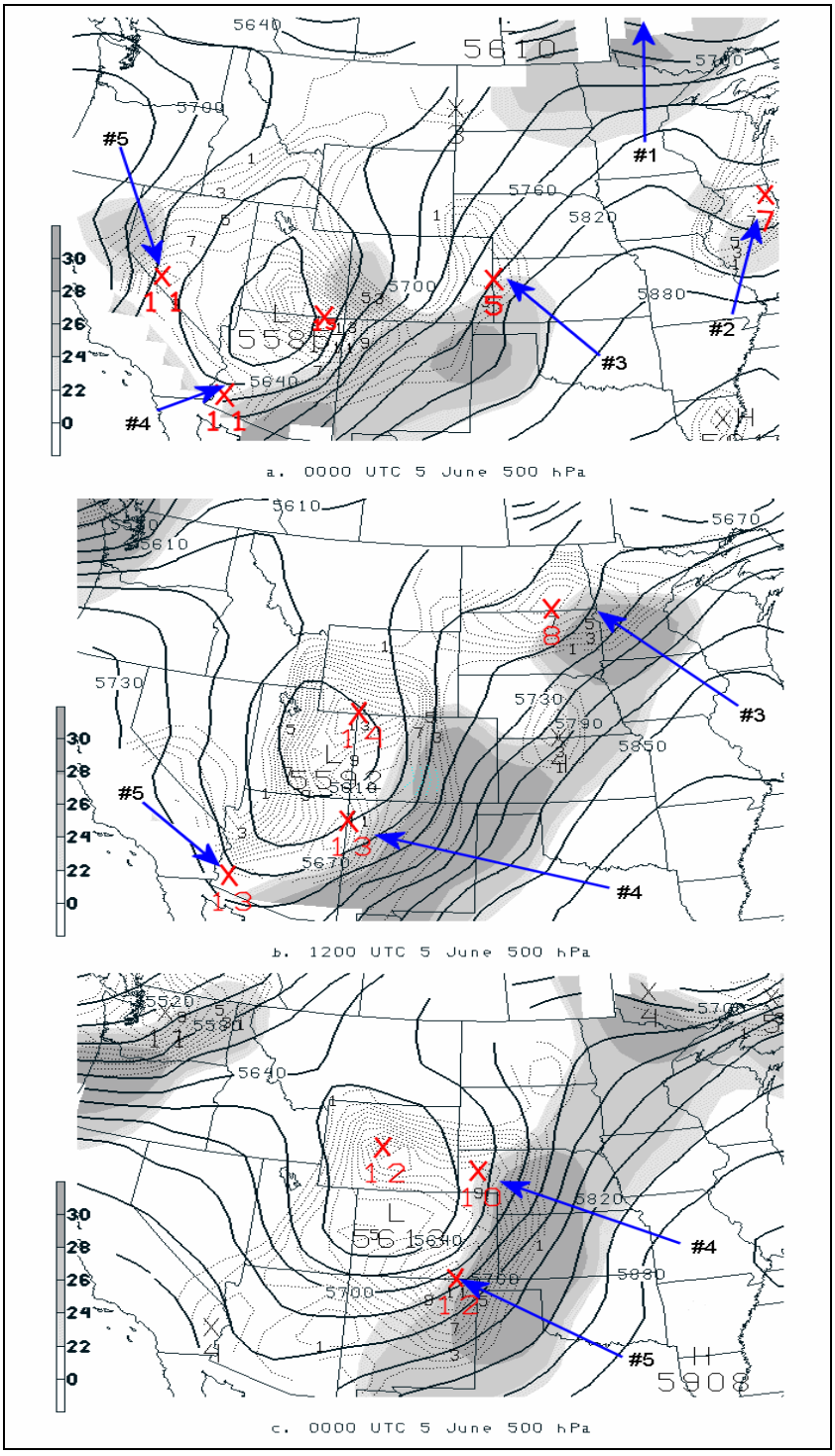

Figure 12. Objective 500 hPa analyses. Heights are thick solid lines, contoured every 30 m. Thin dashed contours are vorticity in s^{-1}. Shading is isotachs in m s^{-1} from 22 to 30. Individual shortwave troughs are indicated in red and labeled from #1 to #5. (a) is 0000 UTC 5 June, (b) is 1200 UTC 5 June, and (c) is 0000 UTC 6 June.

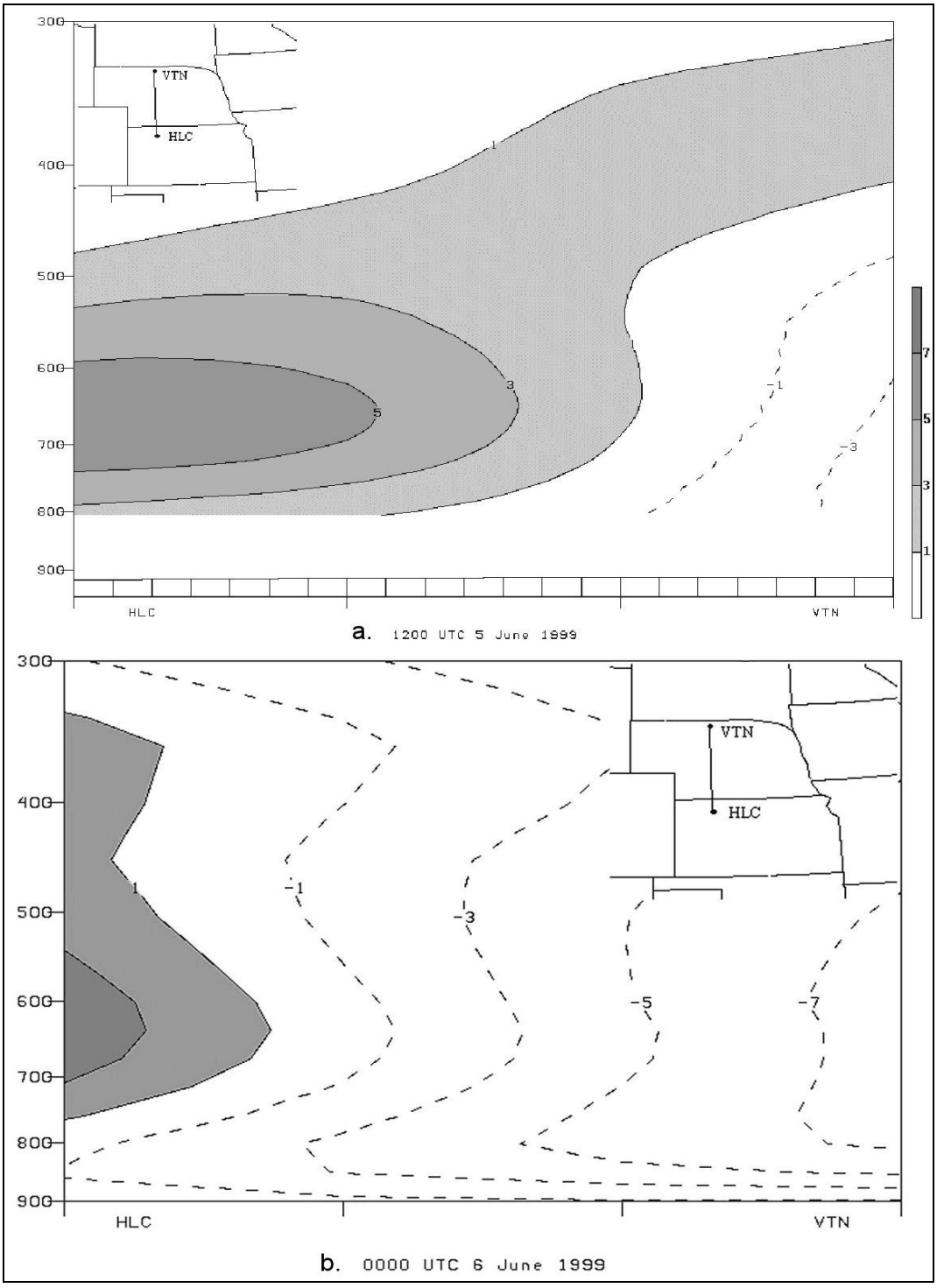

Figure 13. Cross-section analysis at 1200 UTC 5 June (a) and 0000 UTC 6 June (b) using gridded observed data. Cross-section is from Hill City, KS (HLC) to Valentine, NE (VTN). Contours are omega in μbar s^{-1}. Positive values indicate regions of subsidence.

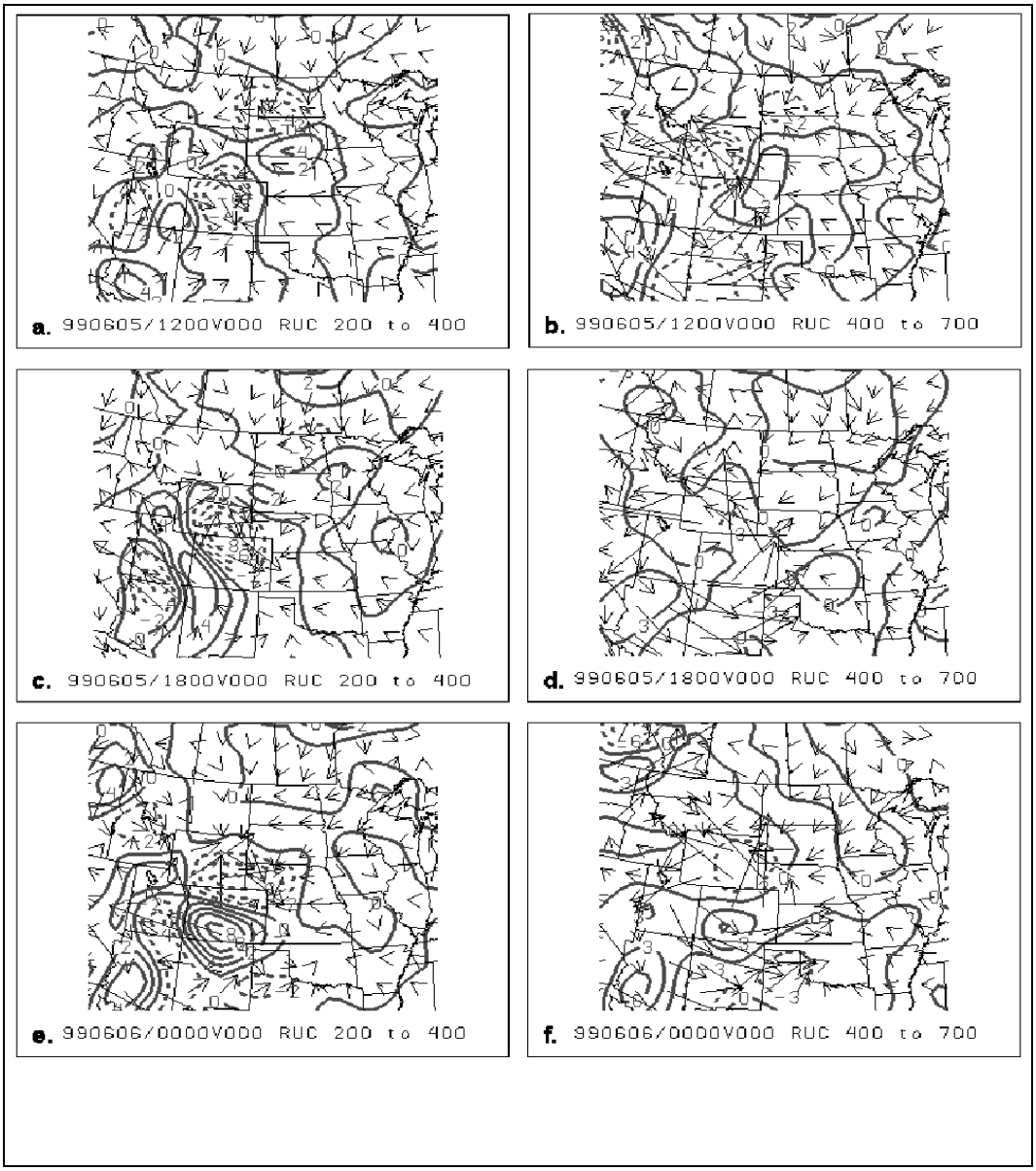

Figure 14. RUC Q-vectors and Q-vector divergence (10^{14} K m^{-2} s^{-1}) for the upper (200 to 400) and mid levels (400 to 700) using a smoothed height field. (a) and (b) are from 1200 UTC 5 June, (c) and (d) are from 1800 UTC 5 June, and (e) and (f) are from 0000 UTC 6 June. Solid contours indicate areas with support for large scale subsidence. Dashed contours indicate areas supportive of large scale upward vertical motion.

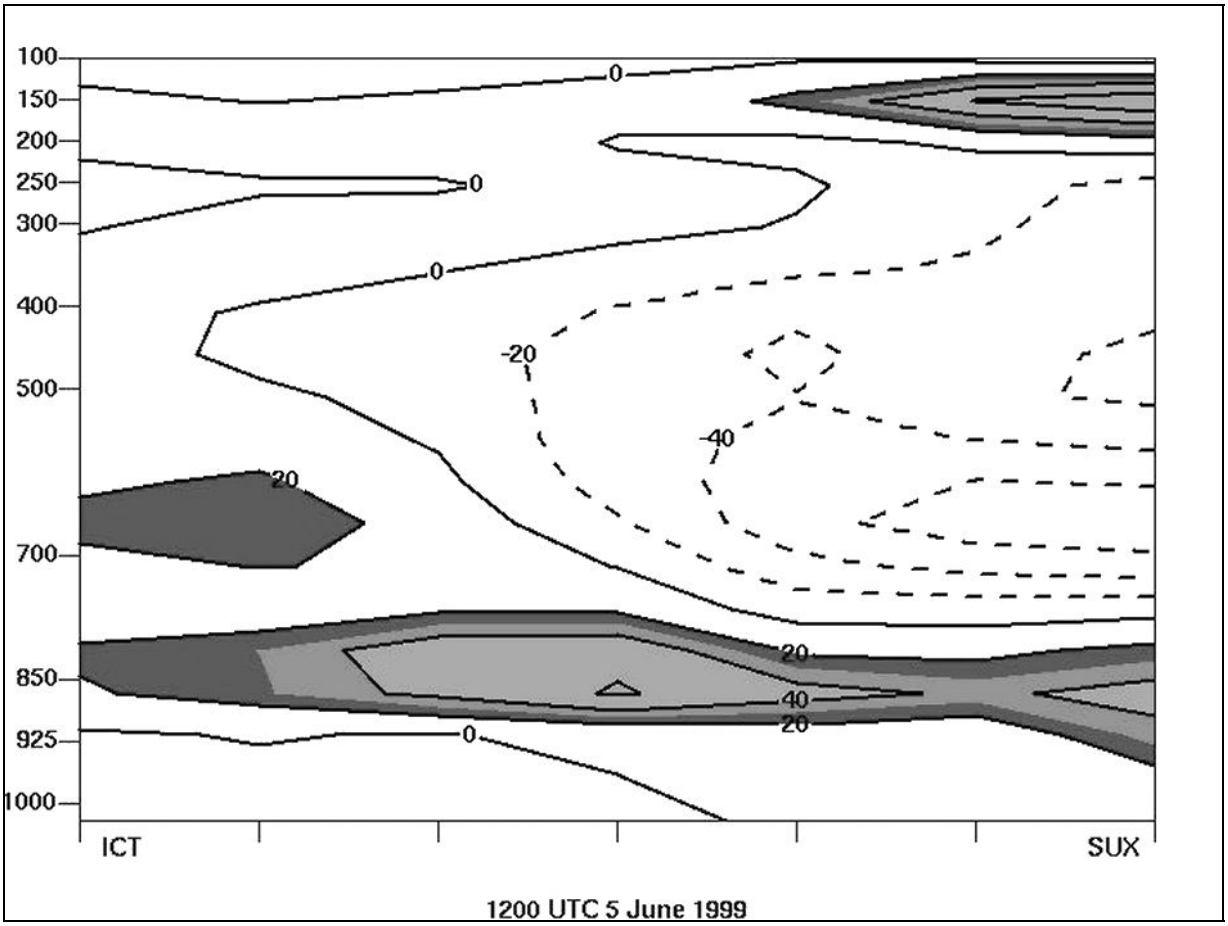

Figure 15. Cross-section analysis at 1200 UTC 5 June using gridded data. Cross-section is from Wichita, KS (ICT) to Sioux City, IA (SUX). White contours are Θ_e with units in °C 12hr^{-1}. Shading indicates areas of moisture advection greater than 20 °C 12hr^{-1}.

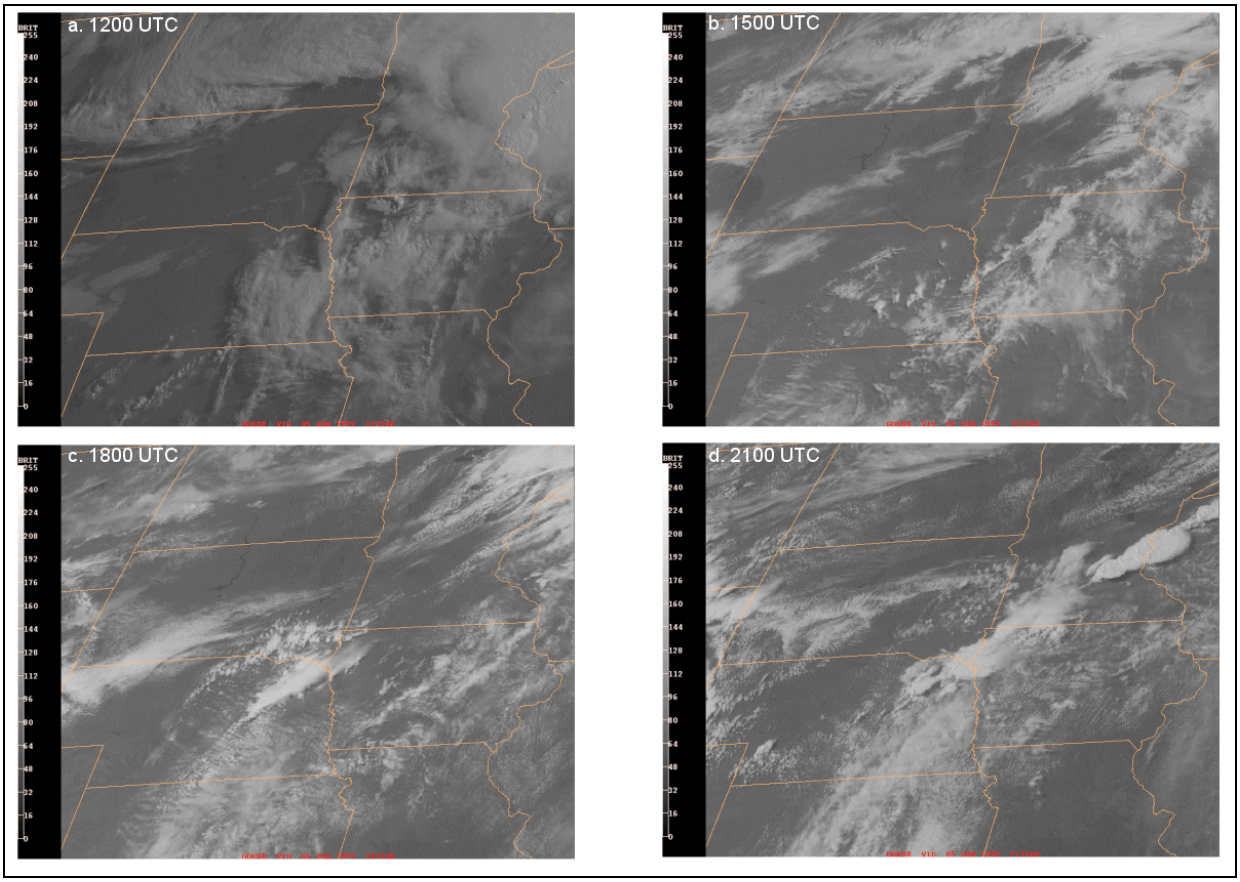

Figure 16. GOES-8 visible satellite images from (a) 1200 UTC, (b) 1500 UTC, (c) 1800 UTC, (d) 2100 UTC.

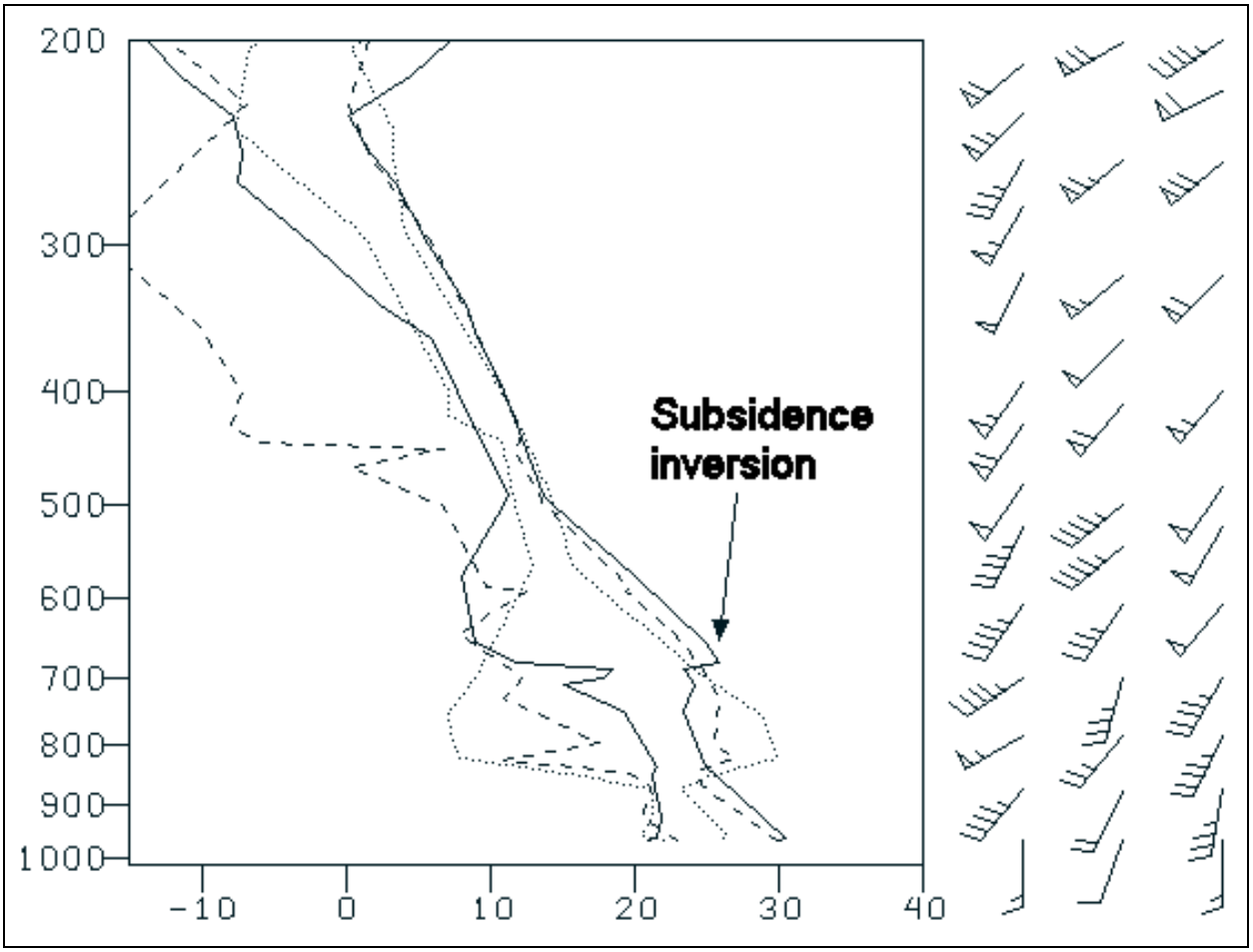

Figure 17. Overlays of the 1200 UTC, 1800 UTC 5 June, and 0000 UTC 6 June soundings from Omaha, NE (OAX). Dotted line and wind column 1 is 1200 UTC. Dashed line and wind column 2 is 1800 UTC. Solid line and wind column 3 is 0000 UTC. Wind is in m s^{-1} (long barb = 5 m s^{-1}, short barb = 2.5 m s^{-1}).

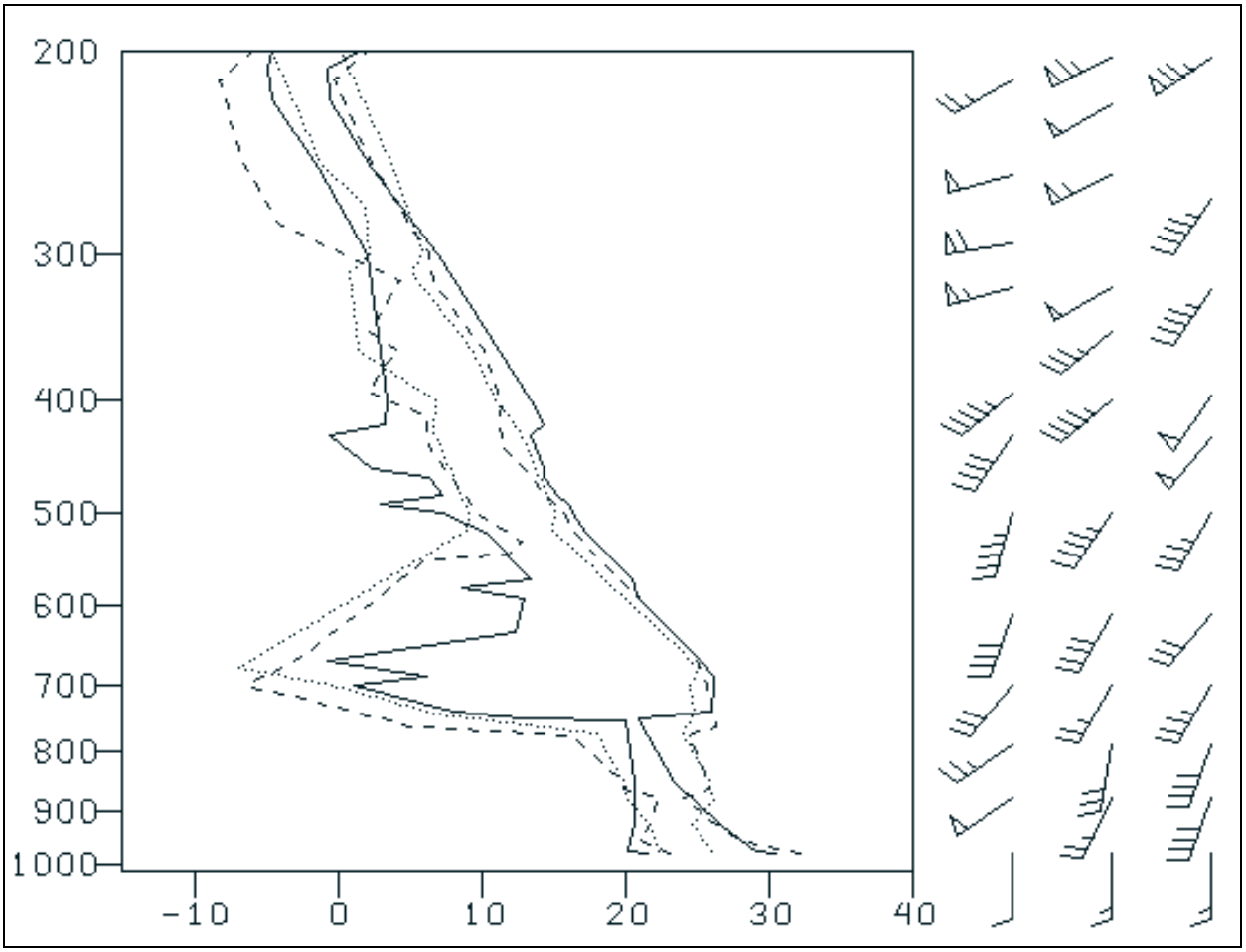

Figure 18. Same as Fig. 17 for Topeka, KS (TOP).

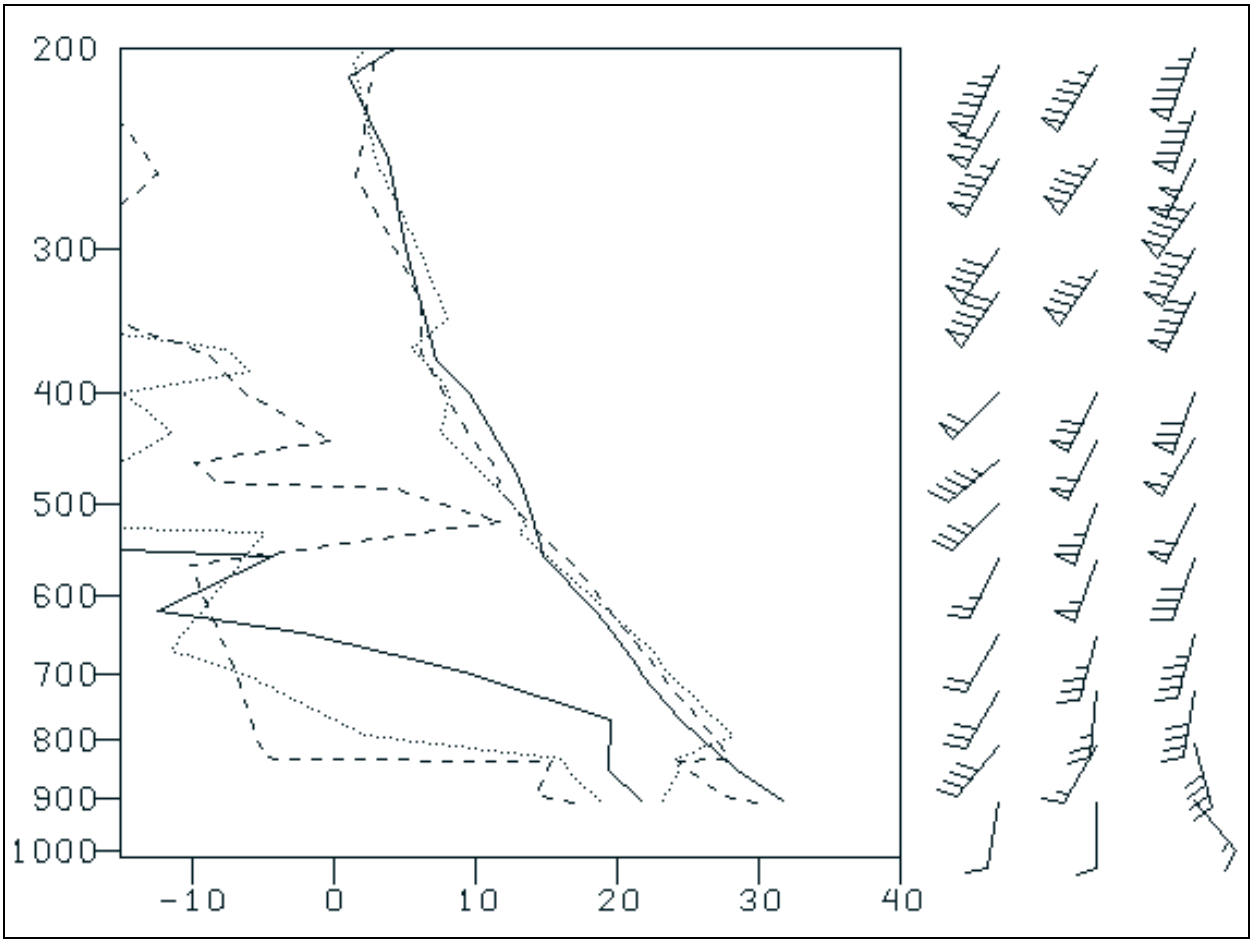

Figure 19. Same as Fig. 17 for North Platte, NE (LBF).

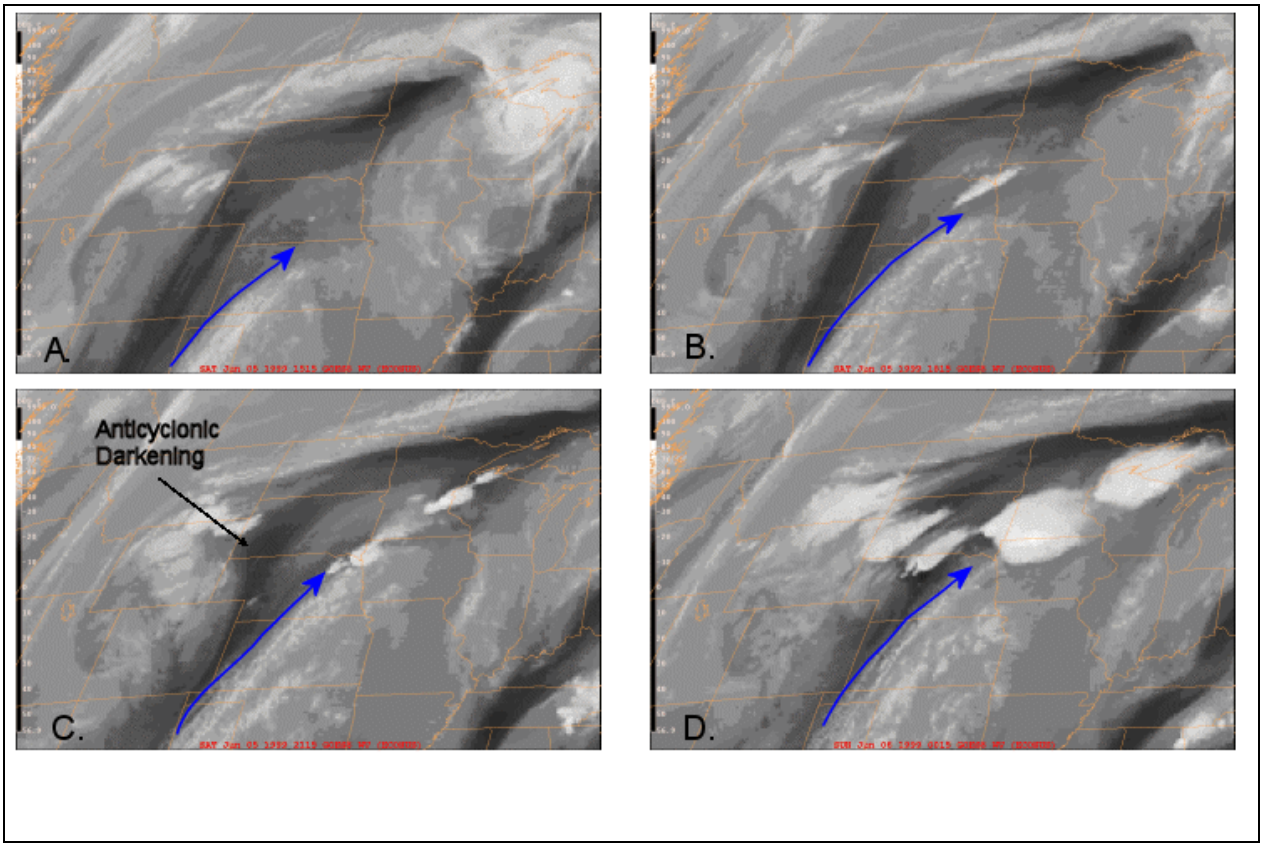

Figure 20. GOES-8 water vapor (6.47-7.02 µm) for (a) 1515 UTC, (b) 1815 UTC, (c) 2115 UTC, and (d) 0015 UTC 6 June. Blue arrows denote the progression of the western edge of the subtropical jet.

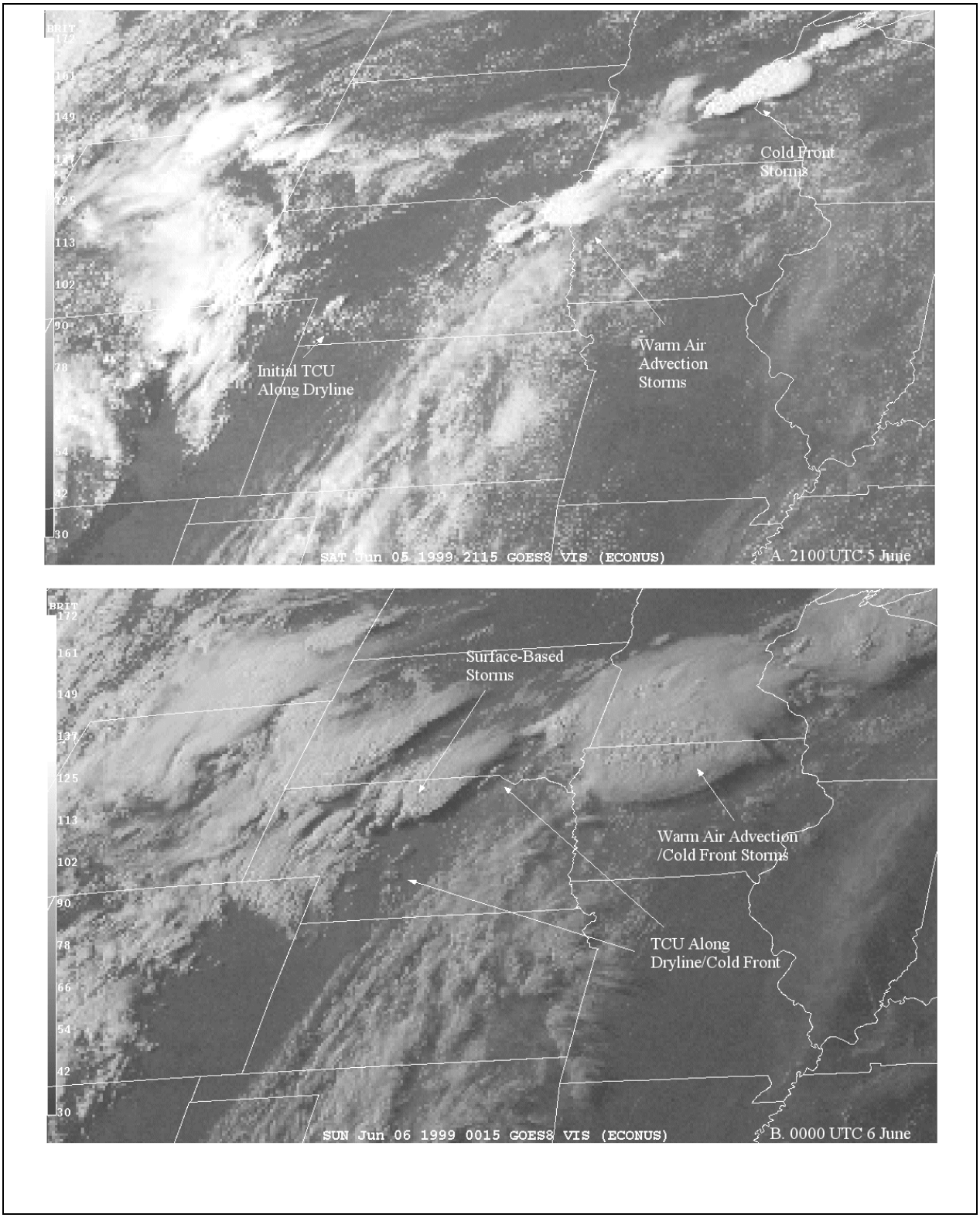

Figure 21. GOES-8 visible satellite imagery from (a) 2100 UTC 5 June and (b) 0000 UTC 6 June.

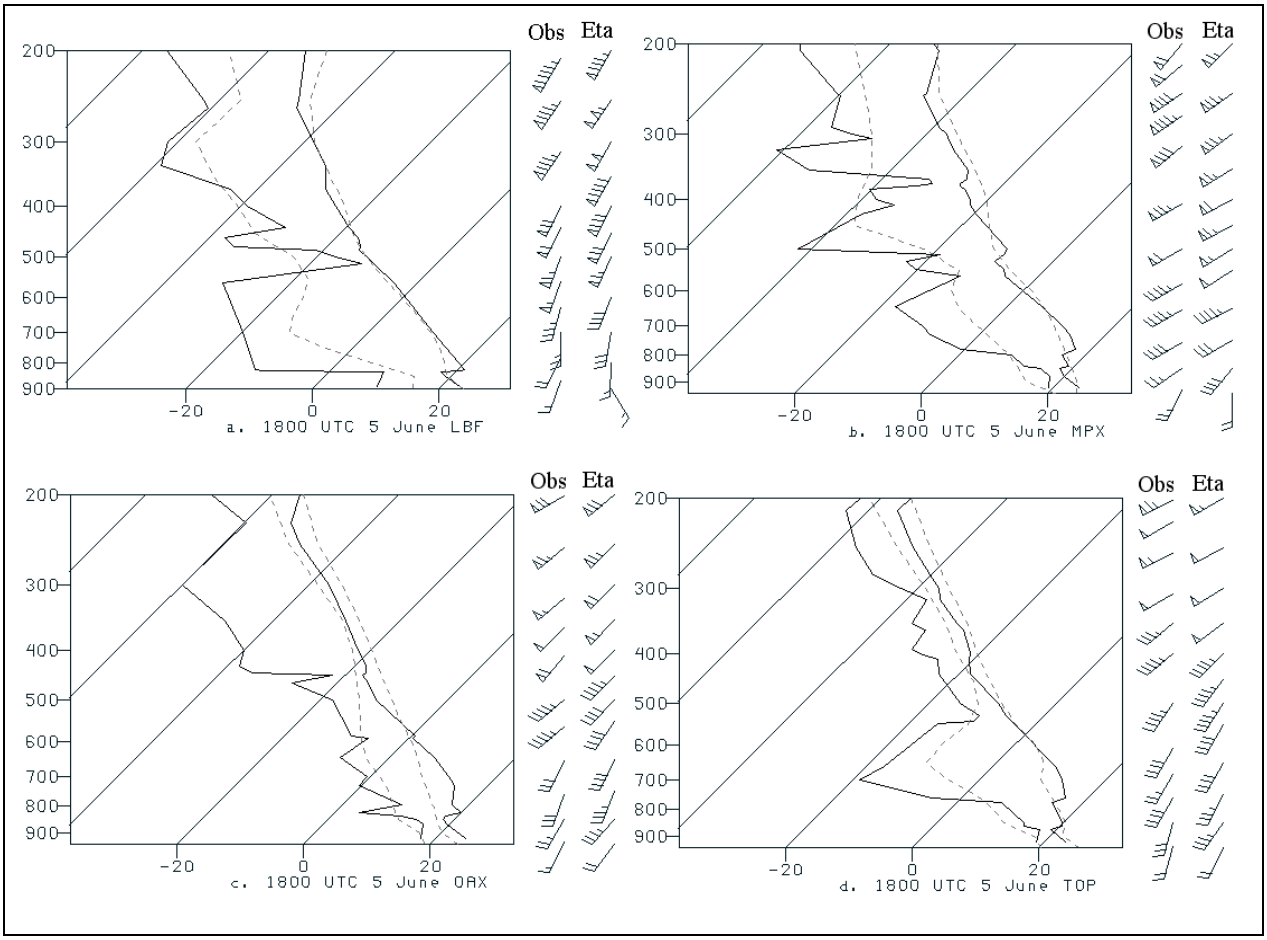

Figure 22. Comparison of the observed (solid) 1800 UTC 5 June soundings and the Eta 6 h forecast soundings (dashed) for (a) North Platte, NE (LBF), (b) Minneapolis, MN (MPX), (c) Omaha, NE (OAX), and (d) Topeka, KS (TOP). Winds are in m s-1 (long barb = 5 m s^{-1}, short barb = 2.5 m s^{-1}).

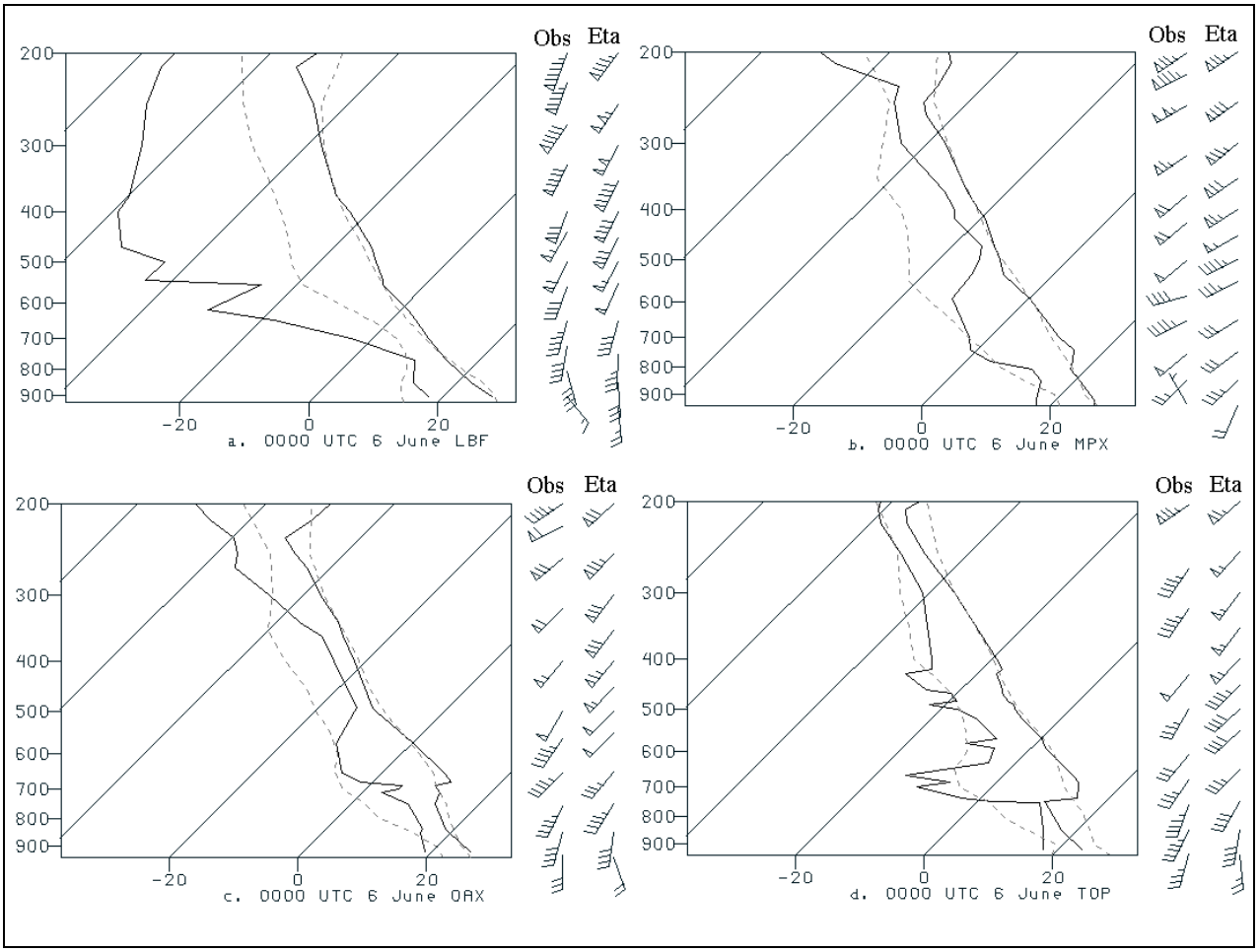

Figure 23. Same as Fig. 20 but for 0000 UTC 6 June.

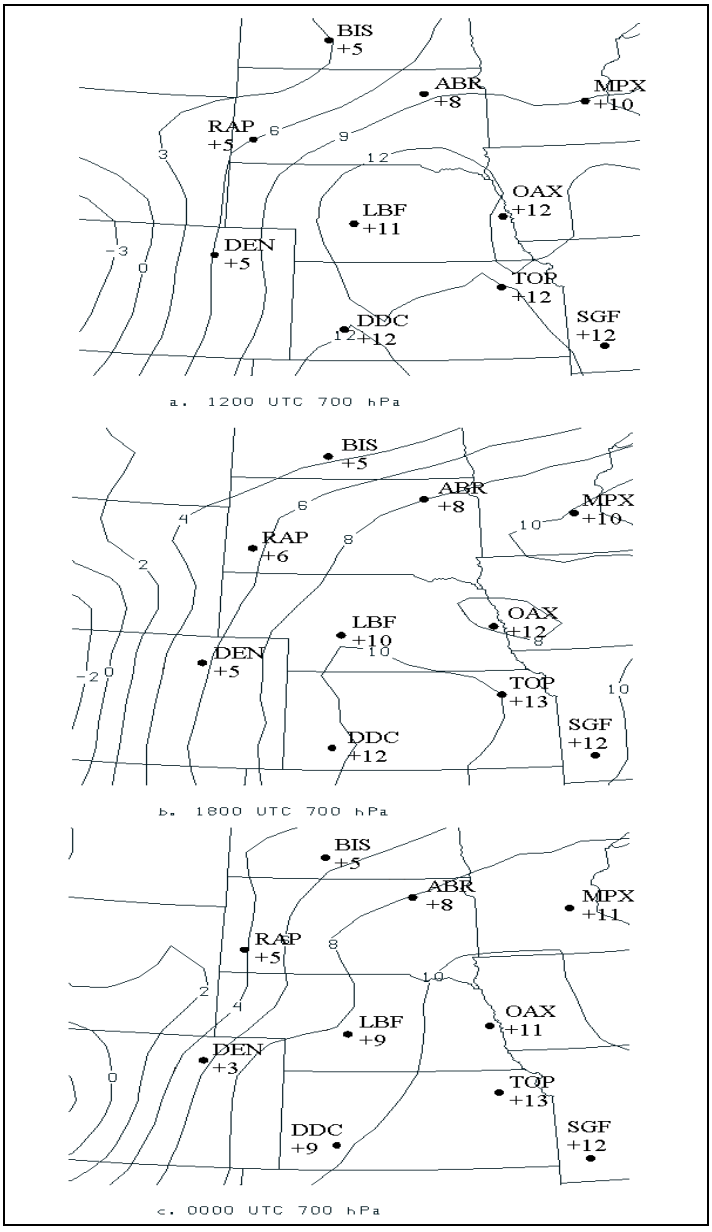

Figure 24. Comparison of observed 700 hPa temperatures, and forecast 700 hPa temperatures from the Eta model (contoured ever 2 EC intervals)for the model analysis (a), 6 hour forecast (b), and 12 hour forecast (c).